Title: Investigating the developmental onset of regenerative potential in the annelid *Capitella teleta*

Authors: Alicia A. Boyd, Elaine C. Seaver

Whitney Laboratory for Marine Bioscience, University of Florida

Corresponding author: Elaine C. Seaver (seaver@whitney.ufl.edu)

Keywords: regeneration, cell division, larva, *vasa*, metamorphosis

Abstract:

An animal's ability to regrow lost tissues or structures can vary greatly during its life cycle. The annelid *Capitella teleta* has robust posterior, but not anterior, regeneration as a juvenile and an adult. In contrast, embryos display only limited replacement of specific tissues. To investigate when during development *C. teleta* becomes capable of regeneration, we assessed the extent to which larvae can regenerate. We hypothesized that larvae exhibit intermediate regeneration potential and demonstrate some features of juvenile regeneration, but do not successfully replace all lost structures. Both anterior and posterior regeneration potential of larvae were evaluated following amputation. Responses were analyzed by EdU incorporation, immunohistochemistry, phalloidin staining, and in situ hybridization. Wound sites were evaluated for re-epithelialization, cell proliferation, stem cell marker expression, the presence of neurites and regrowth of structures. Wound healing occurred within 6 hours of amputation. Cell proliferation at the wound site was observed for up to 7 days following amputation. In addition, the stem cell marker *vasa* was expressed at anterior and posterior wound sites. However, growth of new tissue was observed only in posterior amputations. Neurites from the ventral nerve cord were also observed at posterior wound sites. *De novo ash* expression in the ectoderm of anterior wound sites indicated neuronal cell specification, although the absence of *elav* expression indicated an inability to progress to neuronal differentiation. In rare instances, cilia and eyes reformed. Both amputations induced ectopic expression of the myogenesis gene *myoD*. Our results indicate that amputated larvae complete early, but not late, stages of regeneration, indicating a gradual acquisition of regenerative ability in *C. teleta.* Furthermore, amputated larvae can metamorphose into burrowing juveniles, including those missing brain and anterior sensory structures. To our knowledge, this is the first study to assess regenerative potential of annelid larvae.

1. Introduction

Regeneration is the replacement of tissues or structures after injury or amputation. The ability to regenerate lost tissues varies throughout the animal kingdom (Alvarado, 2000). Animals such as echinoderms can to completely reform any lost structure (i.e., whole-body regeneration) with hardly any restriction. Other animals have a more restrictive capacity to regenerate and reform only specific structures; for instance, limbs in amphibians (Brockes, 1997; Byrnes, 1904; Singer, 1954) or the heart in spiny mouse (Gaire et al., 2021). Finally, there are animals like the leech that display almost no regenerative capability (Özpolat & Bely, 2016).

The capacity to regenerate can also vary throughout an animal's life cycle. Some animals lose regenerative potential as they mature. For example, the *Xenopus* frog has robust regenerative ability to replace tissues (i.e., appendages, nervous system, and heart) as a tadpole (Harrison, 1898), but with age this regenerative ability is progressively lost (Phipps et al., 2020). Other animals gain regenerative potential with age. Crinoids, such as *Antedon rosacea,* have a limited ability to regenerate as larvae, but are capable of whole-body regeneration as adults (C. Carnevali, 2006; M. D. C. Carnevali et al., 1993). Ascidians such as *Ciona* have a more dynamic change in regenerative ability through their life cycle. *Ciona intestinalis* lacks regenerative ability as larvae yet exhibit robust structural regeneration as adults only to progressively lose this ability with advanced age (Jeffery, 2015). Other animals exhibit robust regenerative potential throughout their entire life cycle. For example, sea stars exhibit whole-body regeneration at larval, juvenile, and adult stages (C. Carnevali, 2006). Most published surveys of regeneration ability focus on adult stages, while few studies examine regeneration potential throughout the life cycle. Furthermore, the mechanisms that control changes in regeneration abilities across the life cycle are unknown. This historically narrow focus may be expanded by appraising larval regeneration in a range of indirect developing animals.

Annelids are segmented worms that, as a phylum, have a wide range of documented regenerative abilities as adults. There are worms that lack the ability to regenerate following transverse amputation, have partial regeneration (e.g., anterior or posterior only), or undergo whole-body regeneration (A. E. Bely, 2006). A systematic review of regenerative ability revealed that anterior and posterior regeneration are widespread across the phylum, alongside numerous examples of loss of regeneration (A. E. Bely, 2006). Furthermore, it is likely that both anterior and posterior regeneration are ancestral for adult annelids (Zattara & Bely, 2016). It is not known if such a range of regeneration potential exists at other stages of the annelid life cycle. To our knowledge, a broad assessment of larval regenerative potential is lacking for annelids.

Several features of *C. teleta* biology make it an excellent choice for contributing to research of regeneration potential across the lifespan. First, previous studies indicate there is a change in the regeneration ability across the life cycle of *C. teleta*. Juvenile and adult worms are capable of robust posterior regeneration (de Jong & Seaver, 2016; Giani et al., 2011). In contrast, early-stage embryos generally do not regulate following the laser deletion of individual cells (Pernet et al., 2012) (apart from eye and germline precursor cells (Dannenberg & Seaver, 2018; Yamaguchi et al., 2016)). It is not currently known when *C. teleta* gains its structural regenerative ability, or to what degree larvae might be capable of regeneration. Second, worms can be maintained in the laboratory and bred throughout the year, providing consistent production of embryos, larvae, and juveniles for experimentation. Since the sequencing of the *C. teleta* genome (Simakov et al., 2013), many tools are now available for experimental manipulation in this animal. Methods for analyzing spatiotemporal gene expression such

as in situ hybridization, antibody labeling, and cell fate maps are well-established and readily available (Meyer et al., 2010).

We sought to determine when regeneration potential is initiated during the life history of *C. teleta.* We hypothesized that *C. teleta* larvae may have limited regeneration potential distinct from juveniles and adults. We anticipated that limited potential would manifest itself as displaying early stages of regeneration without successfully replacing lost tissues and structures. Such a scenario would suggest that *C. teleta* acquires its regenerative ability gradually through its life cycle. Alternatively, the onset of regenerative potential may coincide with metamorphosis. Such a rapid shift would be indicated by a complete lack of regenerative features in larvae. To test our hypotheses, we developed an amputation protocol for larvae to investigate both anterior and posterior larval regeneration. We characterized responses of *C. teleta* larvae to amputation by making direct comparisons with regeneration events in juveniles. At the wound site, we documented epithelial wound healing, utilized EdU incorporation to evaluate cell proliferation, antibody labeling to analyze changes in neuronal organization, and phalloidin staining to visualize the musculature. We also conducted in situ hybridization to analyze the expression of *ash1* and *elav*, neuronal specification and differentiation genes, respectively, as well as *MyoD*, a muscle differentiation gene.

3. Results

3.1 Capitella teleta larval development

Capitella teleta is an annelid with an indirect life cycle that is an emerging model for development and regeneration studies (Seaver, 2022)(Seaver & De Jong, 2021). It is commonly found in muddy estuaries (Cohen & Pechenik, 1999). During embryonic and larval stages, the adult centralized nervous system, musculature, digestive system, and initial segments develop (Meyer et al., 2015). The non-feeding larvae utilize their larval-specific cilia to swim, aiding in dispersal. Competent larvae metamorphose into burrowing juvenile worms, which reach sexual maturity after approximately 8 weeks.

C. teleta juveniles successfully regenerate in the posterior direction (de Jong & Seaver, 2016). There are three conserved sequential stages of regeneration: wound healing, cell proliferation, and differentiation of new tissues. Following amputation, juveniles wound heal in 4–6 hours and thereafter form a blastema (Fig 1A) (de Jong & Seaver, 2016). Neuronal projections extend from the ventral nerve cord (VNC) into the wound site as early as 2 days post amputation (dpa) in amputated juveniles (Fig 1B), consistent with previously published research (de Jong & Seaver, 2016). In these regenerating juveniles, the thickness of the connective nerve decreases dramatically at the point of amputation, with multiple thin neural projections extending from the old VNC tissue into the wound tissue and thereafter into the blastema/new tissue. This change in the thickness of the VNC can be used as an indicator of the position of the cut site. A localized area of cell proliferation is also observed at the wound site 2 dpa and persists for several days as new segments are formed (de Jong & Seaver, 2016). The musculature, as visualized by phalloidin staining, shows an abrupt change in density of the circular and longitudinal muscle fibers at 3 dpa (Fig 1C); this change in density aligns with the cut site (designated by the acetylated tubulin labelling of the VNC). Specifically, there is a lack of circular muscle and few longitudinal muscle fibers between the old tissue and phalloidin-positive fibers at the posterior end of the animal. Distal to this area of reduced muscles, there is a circular muscle associated with the anus in the new tissue (Fig 1 C).

After approximately 7 days, a new pygidium and additional segments are formed with organized ganglia, peripheral nerves, muscles, gut, and other differentiated tissues (de Jong & Seaver, 2016). Although juveniles are capable of robust posterior regeneration, it is currently unclear to what extent the larvae are capable of regenerating.

The development of *C. teleta* is indirect and begins as eggs are laid in a maternal brood tube. Following embryogenesis, non-feeding larvae develop and remain in the brood tube until they are competent to undergo metamorphosis (Cohen & Pechenik, 1999; Dannenberg & Seaver, 2018). A previously described staging system uses morphological features to identify 9 distinct stages (Seaver et al., 2005). Stages 1–3 describe embryonic development, namely fertilization, cleavage, and gastrulation. Stages 4–9 describe larval development. The transition to a larva in Stage 4 is denoted by the emergence of trochal ciliated bands that divide the body into three regions along the anterior–posterior axis: the head, the segmented trunk, and the pygidium. The prototroch separates the head from the trunk and the telotroch separates the trunk from the pygidium (Fig 1D, E) (Seaver et al., 2005). These two ciliary bands are composed of long cilia. A third ciliary band, the neurotroch, runs along the ventral midline of the trunk and is composed of short cilia. Short cilia are also present in the pygidium. Larvae utilize these ciliary bands to swim in the water column.

As larvae develop (Stages 6 – 9), tissue types differentiate. *C. teleta* has a centralized nervous system with a ladder-like ventral nerve cord (VNC) positioned along the midline of the trunk (Meyer et al., 2015; Seaver et al., 2005). The VNC connects with the brain in the anterior of the head (Meyer et al., 2015). During these stages, musculature is organized segmentally with circular and longitudinal muscles. Two pigmented eyes are located laterally, just anterior to the prototroch (Meyer et al., 2015; Yamaguchi et al., 2016). Gut organogenesis is one of the most visibly pronounced set of changes that occurs between Stage 6 and Stage 9. The foregut is comprised of the mouth (located posterior to the prototroch, along the ventral midline), buccal cavity, pharynx (developed in Stage 7), and esophagus (Boyle & Seaver, 2008). In Stages 8–9, the mid- and hindgut differentiate, becoming olive green and stereotypically coiled by Stage 9 (Fig 1E). In addition, Stage 6 and Stage 9 larvae differ significantly in shape; Stage 6 larvae are elliptical (Fig 1D) and become elongated over time into a rod-like form by Stage 9 (Fig 1E). Stage 9 concludes larval development when larvae become competent to undergo metamorphosis (Seaver et al., 2005).

3.2 Larval amputations

To assess the regenerative potential of *C. teleta* larvae, amputation sites were selected on Stage 6 larvae for both anterior and posterior amputations (Fig 2A). Cut sites for anterior amputations were located just posterior to the prototroch, removing the head and anterior third of the animal (i.e., brain, eyes, and prototroch). Cut sites for posterior amputations were located posterior to where the width of the trunk decreases and slopes to the pygidium, effectively removing the posterior third of the animal, including the posterior growth zone, telotroch and pygidium.

Successful wound healing was identified as the closure of the wound by contraction of the severed edges of the body wall resulting in a continuous epithelial layer at the wound site. To assess wound healing in amputated larvae, we analyzed larvae fixed at 2 hours post amputation (hpa), 3 hpa, 5 hpa, and 6 hpa for an epithelial layer covering the wound site. For anterior amputations, we observed consistent wound healing 6 hpa (Fig 2B) (n = 54/54). For posterior amputations, we observed wound

192 healing as early as 2 hpa (n = 3/15); however, in most cases successful wound healing occurred around 6
193 hpa (Fig 2C) (n = 48/51).

194 Larvae survived multiple days following amputation (i.e., up to 5 dpa in anteriorly amputated
195 animals and up to 7 dpa in posteriorly amputated animals). Furthermore, posteriorly amputated larvae
196 continued to develop on schedule relative to uncut animals (Fig 2D, 2E). For example, chaetae were
197 present by 1 dpa (comparable to Stage 7), pigmented gut appeared by 2 dpa (comparable to Stage 8),
198 and the midgut became coiled by 3 dpa (comparable to Stage 9). Anteriorly amputated larvae also
199 developed chaetae and a pigmented midgut, but the curvature of midgut—a hallmark of Stage 9 larvae
200 (Boyle & Seaver, 2008; Seaver et al., 2005) was delayed by a day. Another difference between anterior
201 and posterior amputations was a difference in shape at the cut site: a blunt end was frequently
202 observed in anterior amputations (Fig 2D) whereas a rounded tapering of tissue was observed distal to
203 the cut site in posterior amputations (Fig 2E). The tapered shape in posterior amputations is different
204 from the shape of the wound site in aged-matched individuals (Stage 9) fixed only 6 hpa. In addition,
205 there was a clear difference in the distance between the posterior edge of the pigmented midgut and
206 the posterior end of most animals 2 dpa–7 dpa due to the presence of mesodermal tissue (compare Fig
207 2E, F).

208 *3.3 Cell proliferation*

209 One key feature of regeneration is the birth of new cells in the region of the wound site. We
210 used age-matched larvae as controls to distinguish between normal growth and an amputation
211 response. Stage 6 larvae have a characteristic pattern of EdU incorporation with limited dividing cells in
212 the anterior ectoderm and anterior mesoderm surrounding the mouth and foregut as well as in the
213 telotroch and pygidium. There are many EdU+ cells in the trunk straddling the midline (Fig 3A). A similar
214 pattern is observed in Stage 7 larvae (Fig 3B). By Stage 9, EdU+ cells are not ordinarily observed, apart
215 from a few cells in the gut and posterior growth zone (PGZ) (Fig 3C, 3D).

216 Anterior amputations show EdU incorporation near the amputation site. The initial pattern of EdU
217 incorporation in anterior amputations (6 hpa) is similar to the pattern observed in age-matched, uncut
218 controls (Fig 3E, 3I). However, by 3 dpa, EdU+ cells are localized near the wound site of the amputated
219 animals in the anterior ectoderm and occasionally in the mesoderm (Fig 3G). EdU+ cells near the wound
220 site persisted through 5 dpa in anterior ectoderm and mesoderm (Fig 3H). In contrast, there is a notable
221 lack of EdU+ cells in the corresponding body region of unamputated animals (Fig 3C, 3D). The ratio of
222 EdU+ cells to nuclei is higher in amputated animals at 3 dpa and 5 dpa at the respective amputation sites
223 compared to uncut controls (Table 1). There is a significant difference between the number of EdU+ cells
224 in the anterior section of 3 dpa and 5 dpa larvae when compared to age-matched, uncut controls (One-
225 way ANOVA test) (Fig 3M).

226 Posterior amputations also show EdU incorporation localized near the wound site. While the pattern
227 of EdU incorporated cells at 6 hpa appears similar to that observed in Stage 6 uncut controls (Fig 3I),
228 there is a progressive shift toward localized expression in amputated larvae. Animals at 1 dpa have
229 fewer EdU+ cells in the anterior 2/3 of the body (Fig 3J) in comparison with uncut Stage 7 controls. By 3
230 dpa, EdU incorporation is not detected throughout the anterior 2/3 of the body, and EdU+ cells are
231 restricted to the area surrounding the cut site (Fig 3K). This localized pattern of EdU incorporation
232 persists through 5 dpa (Fig 3L). In both cut and uncut larvae, the number of EdU+ cells decrease over

time in the anterior and middle sections of the animal. However, cut larvae have more EdU+ cells in the posterior region than the uncut controls (Table 2). The number of EdU+ cells in posterior sections of 3 dpa and 5 dpa larvae is significantly higher compared to age matched, uncut controls (One-way ANOVA test) (Fig 3N). Additionally, there is a higher ratio of localized EdU+ cells/nuclei in posterior amputated larvae than in anterior amputations. Together, this data shows that there is a marked increase in cell proliferation at the wound site following both anterior and posterior amputations.

3.4 Expression of the stem cell marker vasa

To further characterize the larval response to amputation, expression of the stem cell marker *vasa* was analyzed (Dannenberg & Seaver, 2018; Juliano et al., 2010) by in situ hybridization. In uncut larvae, *vasa* is expressed in a dynamic pattern from Stage 6 through Stage 9 (Dill & Seaver, 2008). In Stage 6 larvae, there is expression in the foregut, the PGZ, and in the mesoderm of the trunk (Fig 4 A). By Stage 8, expression is restricted to the foregut, the multi-potent cell cluster (MPC), and the PGZ (Fig 4B). This pattern continues through Stage 9 (with some variability in detection of the MPC) (Fig 4C).

Six hours after anterior amputation, the *vasa* expression pattern in both amputation groups is very similar to the observed pattern in uncut controls (Fig 4D). By 2 dpa, there is *de novo* expression in the anterior ectoderm at the amputation site of anteriorly cut larvae (Fig 4E). By 5 dpa, expression at the wound site is no longer detected, although expression in the MPC and PGZ persists (Fig 4F). In posterior amputations at 2 hpa, trunk mesodermal expression is continuous from one side of the animal to the other and wraps around the posterior end of the body (Fig 4G). We interpret this expression along the posterior face of the animal to be the result of wound healing that pulls the two lateral trunk domains of expression together. At 2 dpa, *vasa* is expressed in the posterior mesoderm and ectoderm near the wound site (Fig 4H). This expression near the wound site is also detectable 3 dpa (Fig 4I) and 4 dpa (data not shown). In summary, we detect *vasa* expression at the wound site 2–3 dpa for both anterior and posterior amputations.

3.5 Generation of new tissue

With the presence of localized cell proliferation at the wound site (Fig 3G, 3H, 3K, and 3L) and what appears to the be growth of new tissue (Fig 2E), the tissue surrounding the wound site was investigated in more detail. To distinguish between pre-exiting tissue and new tissue, the location of the cut site was determined using the nervous system and musculature as markers. We used a framework commonly used for identifying the cut site in juvenile worms with anti-acetylated tubulin marking the nervous system (Fig 1B). An abrupt change in the thickness of the connective nerves, multiple thin extensions from the VNC to the posterior end of the body, and/or unpaired neuronal fibers were indications of a cut site (Fig 1B, 5B, and 5B'). An abrupt decrease in the density of muscle fibers also indicated the location of the cut site (Fig 1C, 5B and 5B"). In many cases, there was a precise concordance in position between an abrupt change in muscle fiber density and thickness of connective nerves. Therefore, using these two markers, we could consistently identify the location of the cut site.

The identification of the cut site allowed us to identify and quantify the presence of new tissue distal to the amputation site in amputated larvae. No evidence of significant growth of tissue in anterior amputations between 6 hpa and 3 dpa was detected (see Table 3). In contrast, there was significant growth in posterior amputations between 6 hpa and 5 dpa. Additional measurements of posterior amputations indicated a significant change in body width (body width at the mouth compared to

immediately posterior to the cut site) between 6 hpa and 5 dpa. This information is consistent with the presence of new growth in posterior amputations. While the position of the cut site indicated by muscle and nerves indicated new growth, there was one measurement that did not. Measurements from the posterior end of the pigmented gut to the posterior of the animal for both the 6 hpa stage 9 and 5 dpa larvae did not show a significant difference between these two groups.

We next characterized the nervous system and musculature of the tissue distal to the cut site. Similar to that observed in 6 hpa control larvae (Fig 5C), anterior amputations in 3 dpa larvae lacked clear evidence of neurites and muscle fibers distal to the wound site (Fig 5 D–D”). In posteriorly amputated larvae, there were also cases in which there was seemingly no change in the larval nervous system (Fig 5G; n = 165/395). Cases in which new growth was not observed lend confidence to those instances when we observed processes distal to the cut site (compare Fig 5F and 5G). In 2 dpa posteriorly amputated larvae with a discernable cut site and new growth, neuronal projections distal to the amputation site were observed that were not detected in 6 hpa larvae (Fig 5E, E’, F). At 5 dpa, nerve processes persist in tissue distal to the cut site (Fig 5I, 5I”). These longitudinal nerve processes are located at the midline and span the length of the new tissue. Additionally, there were circumferential processes that are similar to the orientation of peripheral nerves (Fig 5I”). These processes are oriented medial to lateral, extending from the midline. The entire region of the new tissue has lower density of muscle relative to the preexisting tissue (Fig 5H, 5I’). The fibers that are present are predominately longitudinal muscle fibers. In many cases, individual longitudinal muscle fibers appeared to be continuous with fibers in the preexisting tissue that extend through the amputation site (Fig 5I’, arrow). A phalloidin positive fiber with a circular orientation muscle was occasionally observed posterior to the amputation site. This phalloidin positive fiber is reminiscent of a serotonin positive fiber beneath the telotroch in uncut animals (Meyer et al., 2015); however, a ciliary band was not seen in amputated larvae. A similar arrangement of muscle and nerve fibers in the tissue distal to the amputation site persists through 7 dpa (data not shown). In conclusion, new growth was not observed in anteriorly amputated larvae, but in posteriorly amputated larvae, new growth along with changes in the nervous system and musculature was observed.

3.6 Neural specification and differentiation

Next, we sought to determine if the neural and muscle cell types we observed distal to the amputation site were the result of birth of new cells. We rationalized that the expression of molecular markers of cell fate specification and differentiation in the tissue distal to the amputation site would indicate birth of new cells. For the nervous system, gene expression patterns of neural specification (*ash1*) and neural differentiation markers (*elav*) were analyzed (Meyer & Seaver, 2009). In *C. teleta*, *ash1* is a marker of neural specification during initial neurogenesis of the brain and VNC (Meyer & Seaver, 2009; Sur et al., 2017). In Stage 6 larvae, *ash1* is expressed in the brain, foregut, PGZ, and the pygidium (Fig 6A). By Stage 9, *ash1* expression is restricted to the foregut and PGZ (Fig 6B). In anterior amputations, the pattern observed at 6 hpa for *ash1* expression mirrors that of uncut Stage 6 larvae, with the notable exception of missing brain expression due to the removal of the head (Fig 6C). In 3 dpa specimens, *ash1* was expressed in both the anterior ectoderm and pharynx (Fig 6D). Expression in the ectoderm can be regarded as *de novo ash1* anterior expression since age-matched, uncut controls lack anterior ectoderm expression (compare panels Fig 6B and 6D, E) (n =32/39). The novel anterior ectodermal expression of *ash1* at 3 dpa was present in a punctate pattern similar to what is observed

during *C. teleta* brain development. In contrast, expression in the pharynx corresponds with expression in age matched uncut controls, albeit with fewer cells.

After observing novel anterior neural specification following amputation, the next step of neurogenesis was analyzed by characterizing the pattern of *elav*, a marker of differentiating neurons. Between Stages 6 and 9 in uncut controls, *elav* expression is restricted to the brain and the VNC (Fig 6F & G). In 6 hpa anterior amputations, *elav* is expressed only in the VNC (Fig 6H). This expression pattern persists through 3 dpa, with no new expression domains observed in amputated animals (n =21/21) (Fig 6I). In the one differing case of the 22 scored, we were not able to definitively score it.

3.7 Amputation induces ectopic MyoD expression

We also examined the expression of *MyoD*, a gene known for a role in muscle specification and differentiation (Zammit, 2017). In uncut larvae, *MyoD* is expressed in the mesoderm of the posterior trunk segments at Stage 6 (Fig 7A); this pattern persists through Stage 9 (Fig 7B). There is a developmental progression from anterior to posterior in the larval trunk, with the more mature segments having an anterior position (Seaver et al., 2005). Thus, *MyoD* is expressed in the younger and newly forming segments. Six hours after both anterior and posterior amputations (6 hpa), expression is restricted to the posterior portion of the trunk (Fig 7 C & E), similar to what is observed in uncut controls. At 7 dpa and 3 dpa, there is a drastic expansion of *MyoD* mesodermal expression along the entire length of the trunk in anterior (Fig 7D) and posterior amputees (Fig 7F), respectively. This ectopic expression is in pre-existing tissue in older segments and includes tissue distant from the wound site in the case of posterior amputations.

3.8 Rare regeneration of differentiated cell types

Following amputations, a few cell types occasionally regenerated, namely the larval eyes and cilia. The larvae have two eyes, with each eye consisting of three cells: a pigment cell (Fig 8A), a sensory cell (Fig 8C), and a support cell (not pictured) (Yamaguchi & Seaver, 2013). The pigment cell is readily visible by its orange pigment granules and the sensory cell can be visualized by immunolabeling with the antibody 22C10 (Yamaguchi & Seaver, 2013). Currently, we are unable to assess the presence of the support cell. In uncut Stage 9 larvae, the pigment cells are located slightly anterior, if not inline, with the prototroch, in a lateral position (Fig 8A). The sensory cell in uncut Stage 9 larvae (Fig 8C) is located immediately adjacent and lateral to the pigment cell and has an axonal projection extending from the cell body to the external surface of the ectodermal epithelium. The pigment and sensory cells were scored as independent characters. Following head amputation, the few regenerated pigment cells observed were variable in location and number (n = 28/420; 3-5 dpa). Additionally, as seen in Fig 8B, pigment cells in amputated larvae were ectopically positioned and in proximity to tissues normally not observed in uncut controls (i.e., midgut). Regenerated sensory cells were also observed in amputated larvae and also exhibited variability in location (n= 8/220, 3 –7 dpa). Axon projections in regenerated sensory cells extended to the outer ectodermal surface of the animals (Fig 8D). There was a higher percentage of cases with regenerated pigment cells (7%) compared with sensory cells (4%) in anterior amputations (Fig 8G). Summation of the total number of pigment cells and sensory cells indicates that at least one cell of the eye regenerated in 6% of cases amputated (n = 36/640).

We were surprised by the appearance of new larval eye cells in *C. teleta* larvae since regeneration of anterior structures is not reported in adults (Yamaguchi & Seaver, 2013). Therefore, we

357 conducted a similar experiment with juveniles. Four-week-old juveniles were amputated immediately
358 anterior to the mouth, removing the eye cells. After screening for successful wound healing and visual
359 inspection that pigment cells were removed, a portion of the amputated juveniles were fixed at 4 hpa
360 and used to confirm the removal of the sensory cells (n =21/21). No pigment cells were observed in
361 amputated juveniles at 7 dpa (n = 0/43). Using 22C10 antibody labelling, a small proportion of cases with
362 eye sensory cells were observed (Fig 8E) (n = 6/43; 14%). Regenerated sensory cells were ectopically
363 located compared to their position in uncut controls (Fig 8E, 8F). Five of the six juveniles with
364 regenerated sensory cells had a small portion of brain present in the anterior of the animal; only one
365 case lacking a brain had a sensory cell. In summary, pigment cells did not regenerate in juveniles,
366 although sensory cells were detected in a small fraction of cases.

367 There are four external ciliated structures in *C. teleta* larvae: prototroch, neurotroch, telotroch,
368 and pygidium. The prototroch and telotroch are composed of relatively long cilia (prototroch cilia length
369 ~25-30 microns and telotroch cilia length ~20-28 microns), and the neurotroch and pygidium have short
370 cilia (neurotroch cilia length ~ 8-10 microns, pygidium length ~5-7 microns) (Fig 9A). At 6 hpa, larvae
371 lacked long cilia at the cut site (Fig 9 B & C), due to amputation of the prototroch and telotroch in
372 anterior and posterior amputations, respectively. In rare cases (n = 12/161), short cilia were observed at
373 the anterior end of anteriorly cut animals at 5 dpa, distal to the amputation site (approximately 8
374 microns in length) (Fig 9E). Long cilia were not observed following anterior amputations (n = 0/161).
375 While rare (n = 22/370), both long (~25 microns) and short (~9 microns) cilia were observed following
376 posterior amputations between 3–7 dpa (Fig 9F).

377 *3.9 Metamorphosis following amputation*

378 *C. teleta* is typically competent to undergo metamorphosis into juveniles as Stage 9 larvae.
379 Metamorphosis is rapidly induced by exposure to vitamin B supplements dissolved in salt water (Burns
380 et al., 2014). To test whether amputated larvae are capable of successfully undergoing metamorphosis,
381 uncut, anteriorly amputated, and posteriorly amputated larvae were exposed to a solution containing
382 vitamin B. Animals were screened for stereotypical signs of successful settlement and metamorphosis
383 following the definition of Cohen and Pechenik (1999). These changes include a loss of swimming
384 behavior and initiation of burrowing behavior, loss of both ciliary bands (telotroch and prototroch), and
385 the appearance of an elongated, worm-like body shape. Uncut, uninduced control larvae swam with
386 their prototroch and telotroch bands intact for the duration of the experiment (Fig. 10A) (2 hr, n =
387 532/534). In contrast, virtually all larvae in the induced, unamputated control group successfully
388 underwent metamorphosis within two hours of exposure, settling on the bottom of the dish, dropping
389 their cilia, adopting burrowing behavior, and extending in length along their anterior-posterior axis (Fig
390 10B) (n = 203/207). Both sets of amputated larvae followed a similar pattern to what was observed for
391 unamputated larvae. Specifically, one day after anterior amputation, larvae either continued to swim in
392 the water column in the absence of a metamorphic cue (Fig. 10C) (n=65/66) or settled to the bottom of
393 the dish and underwent metamorphosis within two hours of exposure to a metamorphic cue (Fig. 10D)
394 (n=135/136). Similarly, individuals whose posterior ends had been removed retained their prototrochal
395 bands and continued to swim in the absence of a metamorphic cue (Fig. 10E, arrow) (n=65/65), yet,
396 underwent rapid settlement and metamorphosis within two hours of exposure (Fig. 10F) (n=143/144).
397 Without an induction cue, amputated laravae continue to swim in the water column and retain their
398 ciliary bands for several days, demonstrating that amputation itself does not induce metamorphosis (Fig

399 9E, F). Together, these results demonstrate *C. teleta* larvae can detect a metamorphic cue and
400 successfully execute metamorphosis in the absence of either anterior or posterior structures.

401 **4. Discussion**

402 *4.1 Limited regeneration in C. teleta larvae*

403 This study demonstrates that the initial events following amputation appear to be quite similar
404 between *C. teleta* larvae and juveniles. Following both anterior and posterior amputation, larvae wound
405 heal in a similar time frame as previously reported for posterior amputation of juveniles (i.e., within 6
406 hpa) (de Jong & Seaver, 2016). Following wound healing, EdU+ cells appear localized at the wound site
407 at 2 dpa in juvenile posterior regeneration, and the number of EdU+ cells increases over time (de Jong &
408 Seaver, 2016). EdU incorporation in anterior-facing wound sites in juveniles of *C. teleta* has not been
409 formally characterized. In both anterior and posterior larval amputations, EdU is incorporated near the
410 wound site 3 dpa and this persists through 5 dpa, comparable to the pattern of EdU incorporation at the
411 wound site in regenerating juveniles. There is a difference in the number of EdU+ cells between anterior
412 and posterior amputations in larvae, with posterior amputations exhibiting more EdU+ cells. One
413 difference in cell proliferation patterns between juveniles and larvae is a change in position of the
414 localized EdU+ cells. During posterior regeneration in juveniles, localization of EdU+ cells progressively
415 shifts anteriorly to a subterminal position, a shift that corresponds with the re-establishment of the
416 juvenile PGZ. We did not observe such a shift in larvae. It is interesting to note that in the annelid
417 *Paranais litoralis*, BrdU is incorporated near the anterior wound site even though these animals have
418 lost the ability to regenerate their heads (Bely and Sikes, 2010). This finding, along with our results in *C.*
419 *teleta* larvae, emphasize that a block in regeneration can occur subsequent to the initiation of cell
420 division at the wound site, and cell division at the wound site is not a reliable predictor of successful
421 regeneration.

422 Interestingly, expression of the stem cell marker *vasa* at the wound site was observed in both
423 sets of amputated larvae. In successful posteriorly regenerating juveniles, *vasa* is expressed locally at the
424 wound site at 2 dpa and persists for several days (de Jong & Seaver, 2017). In larvae, *vasa* expression has
425 a different duration between anterior and posterior amputations. In anterior amputations *vasa*
426 expression is transient; it is detectable at 2 dpa but not 5 dpa. Conversely, localized *vasa* expression is
427 observed at 2 dpa and persists through 5 dpa in posterior amputations. We interpret the localized
428 expression of *vasa* at the posterior wound site as either the result of *de novo* expression or expression
429 maintained from an earlier stage (i.e., 6 hpa). The spatial and temporal patterns of EdU incorporation
430 and *vasa* expression are very similar in posterior amputations. In contrast, near the wound site in
431 anterior amputations, *vasa* expression is of a shorter duration than EdU incorporation. We hypothesize
432 that this difference between anterior and posterior amputations is related to the new tissue growth in
433 posterior amputations yet absent in anterior amputations.

434 Additional features of juvenile posterior regeneration are the presence of neural projections
435 into the wound site and muscle reorganization distal to the amputation site. In juveniles, this
436 phenomenon is observed approximately at 2 dpa (de Jong & Seaver, 2016). In larval posterior
437 amputations, neurites were present distal to the cut site by 2 dpa. However, these neurites were not
438 observed in larval anterior amputations. With respect to muscle fiber organization, there is an abrupt
439 transition between the presence and absence of muscle fibers distal to the cut site in both juveniles and
440 larval posterior amputations that was not observed in larval anterior amputations. We were unable to

441 determine whether fibers present distal to the amputation site in posterior larval amputations resulted
442 from birth of new neural or muscle cells or from the extension of pre-existing cells.

443 To understand the development of the tissue distal to the cut site in larvae, we characterized
444 the specification and differentiation of cell types (i.e., neural cell types and cilia) in amputated larvae.
445 The timing of neural specification or differentiation in juveniles has not been investigated in detail, but
446 differentiated tissues are present by 7 dpa (de Jong & Seaver, 2016). Analysis of *de novo ash1* expression
447 indicates the specification of neural fates in larval anterior amputations. Surprisingly, subsequent
448 differentiation of neural tissues was not detectable, as illustrated by the absence of *elav* expression in
449 larval amputations. Anterior amputation of larvae results in incomplete tissue and structure
450 regeneration—an observation consistent with the response in juveniles to anterior amputations.
451 Despite a general lack of anterior structural differentiation in amputated larvae, we surprisingly
452 observed rare cases in which differentiated eye cells and cilia reappeared within 3–7 dpa. Additionally,
453 sensory eye cells (but not pigment cells) regenerated in juveniles at a higher proportion than in larvae.
454 While rare, we are confident that these cells are regenerated differentiated eye cells in amputated
455 larvae and juveniles. In summary, the beginning stages of regeneration occur in amputated larvae but
456 there is a lack of cell or tissue differentiation. These data indicate that *C. teleta* larvae exhibit limited
457 regeneration abilities relative to the successful posterior regeneration observed in juvenile and adult
458 stages. Additionally, detection of initial stages of regeneration in larvae suggests that *C. teleta* has a
459 gradual transition in regenerative potential, rather than a stark change in potential that corresponds
460 with the onset of metamorphosis.

461 *4.2 Ectopic expression in preexisting tissue*

462 *MyoD* functions in muscle development and its expression in muscle progenitor cells is an indication
463 of myogenesis (Zammit, 2017) (Rawls & Olson, 1997). In response to amputation, *MyoD* becomes
464 ectopically expressed across the length of the larval body in *C. teleta*. This ectopic expression may result
465 in an increase in muscle cell number to compensate for a decrease in body length following amputation,
466 although we did not observe an obvious increase in the number of muscle fibers 3 – 5 dpa. Alternatively,
467 ectopic expression of *MyoD* may be an injury-specific response that leads to cell dedifferentiation and
468 return to a precursor state. Such a precursor cell population may contribute to regenerating tissue. It is
469 notable that the induction of ectopic *MyoD* expression occurs in the absence of a complete regeneration
470 response. Regardless, future functional work is needed to better understand the implications of this
471 novel *MyoD* expression in amputated larvae. Ectopic gene expression in response to amputation has
472 previously been documented in *C. teleta* and other annelids (de Jong & Seaver, 2016; Kozin et al., 2017;
473 Pfeifer et al., 2012; Takeo et al., 2008). However, in most cases, these are positional identity genes and
474 their ectopic expression likely reflects repatterning of the body fragment in response to amputation.

475 *4.3 Metamorphosis following amputation*

476 Amputated larvae can undergo successful metamorphosis. We were surprised to observe
477 metamorphosis following anterior amputations. In other spiralians, it has been hypothesized that the
478 brain and other anterior sensory organs function in the detection and response to metamorphic cues
479 (Chartier et al., n.d., 2018; Conzelmann et al., 2013; Hadfield, 2010; Hadfield et al., 2000). In *C. teleta*, it
480 has been hypothesized that chemo-sensitive ciliated cells in the head ectoderm relay metamorphosis
481 signaling directly to the cerebral ganglia (Biggers & Laufer, 1999). Therefore, we expected that by
482 removing the head, anterior amputees would not undergo metamorphosis. Our results demonstrate

483 that the brain is not required for detecting the metamorphic cue, nor for undergoing metamorphosis in
484 *C. teleta*. Without the sensory structures to detect the metamorphic cue, we would expect cilia to be
485 retained. A recent study in the polychaete *Hydroides elegans* similarly demonstrated that its apical
486 sensory neurons are not necessary for successful metamorphosis (Nedved et al., 2021). Furthermore,
487 our results are consistent with a previous study hypothesizing that the inductive metamorphosis signal is
488 detected by sensory neurons that innervate the dorsal pharyngeal pad of the pharynx (Biggers et al.,
489 2012). In our experiments, the pharynx remained intact in both anterior and posterior amputated
490 larvae. Successful metamorphosis from amputated larvae supports the hypothesis that detection of the
491 metamorphic cue in *C. teleta* can occur in the pharynx.

492 *4.4 Larval regeneration in marine invertebrates*

493 Larval regeneration studies are overshadowed by numerous studies of adult and juvenile
494 regeneration. Of the taxa where larval regeneration is studied, there is a disproportionate emphasis on
495 echinoderms (C. Carnevali, 2006; G. Cary & Hinman, 2017; Oulhen et al., 2016; M. C. L. Vickery et al.,
496 2001; M. S. Vickery & McClintock, 1998; Minako S. Vickery et al., 2002). Larval regeneration has been
497 documented in all classes of echinoderms examined (G. A. Cary et al., 2019; M. C. L. Vickery et al., 2001).
498 Regenerative potential can vary significantly across life stages and age. In some animals, larval tissues
499 and organs have similar regenerative abilities as adults. Asteroids and echinoid larvae have
500 demonstrated the ability to regenerate completely, regardless of developmental stage (C. Carnevali,
501 2006; Minako S. Vickery et al., 2002). In others, like in crinoids, larvae display a limited ability to
502 regenerate. Echinoderms in which larvae have a reduced regenerative ability relative to that of the adult
503 are described as having "attempted" or "limited" regeneration. When regeneration has been recorded
504 in crinoid larvae, it has been described as partial regeneration of body parts in both sessile and
505 swimming larval stages (C. Carnevali, 2006). In contrast, adults are capable of robust structural
506 regeneration even when reduced to 1/5 of the original body size (C. Carnevali, 2006). In the crinoid
507 *Antedon rosacea*, amputated early-stage larvae differ in their regeneration ability compared to late-
508 stage. For early stage amputated larvae, both anterior and posterior halves demonstrate a reduced
509 regenerative capacity. In late-stage larvae, the anterior portions developed typical skeletons, while
510 posterior halves lack stalk development, but have numerous duplicated organs and vestibules (M. C. L.
511 Vickery et al., 2001). Similar to *Antedon rosacea* early-stage larvae, amputation of 2-day old *Holothuria*
512 *poli* into right and left halves resulted in "attempted" regeneration (M. C. L. Vickery et al., 2001). In
513 amputated *Holothuria*, processes similar to development were observed in an amputated coelom in the
514 absence of tissue replacement (M. C. L. Vickery et al., 2001).

515 These cases of limited or attempted regeneration in echinoderms have remarkable parallels with
516 what we documented in *C. teleta* larvae relative to features characteristic of successful regeneration in
517 *C. teleta* juveniles and adults. Amputated larvae (both anterior and posterior amputations) resulted in
518 completed wound healing, localized cell proliferation, and innervation. However, in most cases, we did
519 not observe neural and muscle differentiation, nor the reformation of ciliary bands or other structures.
520 While larvae appear to have the rare capacity to regenerate cilia and eyes, we conclude that complete
521 regeneration is not the typical response to amputation. The initiation of the regeneration response in
522 larvae, but a lack of complete replacement of lost structures is consistent with our hypothesis that
523 larvae have limited regeneration potential. Furthermore, our data do not support an abrupt onset of
524 regenerative potential coincident with metamorphosis in *C. teleta*, although differences between larval

525 and juvenile regenerative potential demonstrate that there is an increase in regenerative potential
526 following metamorphosis.

527 Outside of echinoderms, there are far fewer examples of larval regeneration studies. In the
528 hemichordate *Ptychodera flava*, larvae display a more restricted regeneration ability than adults.
529 Specifically, ventral regions of larvae regenerate better than dorsal regions and posterior segments
530 regenerate better than anterior segments (Luttrell et al., 2018). Another example comes from the
531 nemertean, *Maculaura alaskensis*, which as an adult is capable of posterior regeneration (Hiebert &
532 Maslakova, 2015). During its life cycle, *Maculaura alaskensis* forms a feeding larva that eventually
533 undergoes a catastrophic metamorphosis. Amputations in larvae revealed that younger larvae were five
534 times more likely to regenerate than older larvae (Moss, 2017). This study substantially contributes to
535 addressing that have been, until now, predominately restricted to deuterostomes.

536 *4.5 Future directions*

537 This study demonstrates differences in regenerative ability across developmental stages of
538 *Capitella teleta*. Future studies could investigate differences in physiological, cellular, and molecular
539 responses to amputation between larvae and juveniles. It has been demonstrated that the extent of
540 regeneration in *C. teleta* juveniles and other annelids can fluctuate depending on nutrition intake (de
541 Jong & Seaver, 2016; Zattara & Bely, 2013). Because *C. teleta* larvae are non-feeding, limited energy
542 resources may contribute to their regeneration limitations. This nutrition hypothesis could be tested by
543 two separate approaches. In the first, cells with high yolk content can be targeted for deletion in early-
544 stage embryos to reduce maternally contributed nutrition. Previous work demonstrated that such
545 deletions result in morphologically normal, albeit smaller larvae (Pernet et al., 2012). These larvae would
546 have a reduced nutritional supply. After performing amputations on the smaller larvae, there may be a
547 further reduction in regenerative potential to what was observed in this study. The second approach
548 would involve investigating the regeneration abilities in a different annelid with a feeding larval form. A
549 feeding larva with more nutritional resources may exhibit full regenerative abilities following
550 amputation. Additionally, an annelid with a longer larval period would have more time to complete
551 regeneration following amputation during the early larval period, while also continually feeding.

552 Timing of developmental maturation may also limit regeneration ability and explain differences
553 between larval and juvenile regenerative abilities in *C. teleta*. An example of one such developmental
554 constraint may be in the maturity of stem cells. A previous study proposed that stem cells travel from
555 the MPC cluster to the wound site during juvenile regeneration (de Jong & Seaver, 2017). MPC cells in
556 larvae may be immature, thereby preventing these stem cells from positively contributing to successful
557 regeneration. Specifically, nascent stem cells may not be capable of self-renewal or migration (Juliano
558 et al., 2010), or of contributing to the blastema. The number of cells in the MPC cluster does not
559 increase during larval development (de Jong & Seaver, 2017), suggesting these cells may be quiescent
560 during this time. A heterotopic transplant of a mature MPC cluster from juveniles into larvae would test
561 this hypothesis. We would expect to see an increased regenerative ability in larvae following
562 transplantation.

563 It is yet to be determined whether the amputations performed during larval stages have lasting
564 effects on survival and growth following metamorphosis. It remains to be seen whether juveniles
565 induced from posteriorly amputated larvae redevelop posterior growth zones, can generate additional
566 segments or are capable of posterior regeneration. Future studies could examine the regeneration

potential of juveniles that result from amputated larvae. Additionally, it could be interesting to determine if the juveniles induced from anterior amputated larvae are capable of posterior regeneration in the absence of a brain.

Previous studies have identified a wide range of regeneration abilities in adult annelids. Adult annelids also display differences in regenerative ability with respect to cut site location. For example, in *Chaetopterous pergamentaceus* (Cuvier et al., 1829) (formally *variopedatus*), posterior regeneration occurs following amputation at any segment; in contrast, anterior regeneration does not occur following amputations posterior to segment 15 (Berrill, 1928) (Cuvier et al., 1829). Regenerative success appears to be influenced by species-specific differences, developmental timing, nutritional status, amputation location, or a combination of these. Future studies can characterize the regeneration ability of other annelid larvae, particularly those whose adults have different regenerative potential than that of *C. teleta*. There may a correlation between adult and larval regenerative potential within individual species. For example, there may be anterior regenerative ability in larvae in a species capable of anterior regeneration as an adult. We are intrigued to learn whether larval regenerative ability is as common as adult regenerative ability in annelids. Comparison of *C. teleta* regeneration abilities to other annelids might lead to a better understanding of the role that development has on regeneration.

2. **Materials and Methods**

2.1 Animal Care

As described in previous work, a colony of *Capitella teleta* was maintained in laboratory at 19°C in glass finger bowls filled with mud and filtered sea water (FSW). Using forceps, larvae were dissected from the brood tubes of healthy females. Broods were maintained individually in FSW until the desired age for amputation or treatment.

2.2 Amputations

Amputations were conducted on a 60 mm petri dish lid covered in a methyl cellulose solution (0.3 g methyl cellulose to 15 ml 1:1 solution of 0.37 M $MgCl_2$: FSW. Glass pipettes pulled into thin, flexible, sharp tips capable of slicing were used as amputation tools. Individual broods were isolated and selected when identified as containing Stage 6 larvae following a standard staging system (Seaver et al., 2005). Stage 6 was characterized by yolk in the anterior portion of the larvae, swimming behavior with a positive phototactic response, and lack of chaetae.

Larvae were incubated in 1:1 $MgCl_2$: FSW for 10 minutes. Individual larvae were transferred to an amputation stage (a platform of black dissecting wax (American Educational Products, Fort Collins, CO, USA in the lid of a 35 mm plastic dish) in a 6 % methyl cellulose in a 1:1 solution of 0.37 M $MgCl_2$: FSW, adding additional methyl cellulose as necessary to achieve immobilization. Larvae were amputated with a pulled glass micro-needle in a continuous, downward motion. The positions of amputations were ~1/3 of the body length for anterior amputations and ~2/3 of the body length for posterior amputations. With each amputation, complete separation of body sections was visually noted. Amputated larvae were transferred to a 60 mm petri dish and incubated in 1:1 $MgCl_2$: FSW for a minimum of 1 hour.

605 Larvae were then washed into FSW containing 60 µg/ml penicillin and 50 µg/ml streptomycin (Sigma-
606 Aldrich Co.)(P/S) and incubated at 19°Celsius until the designated time point. P/S FSW was replaced
607 daily, as necessary, while also monitoring for vitality and swimming behavior.

608 For eye amputations, Stage 6 larvae were amputated posterior to the prototroch as described
609 above, and each individual was visually inspected for correct cut site and complete separation of the
610 two tissue fragments. Two-week-old juveniles were prepared for amputation by incubation in 1:1 $MgCl_2$:
611 FSW for 10 minutes. Individual worms were transferred to a wax amputation stage in a drop of 1:1
612 $MgCl_2$: FSW. The worms were amputated immediately anterior to the mouth, removing the eyes and
613 brain. Individual worms were visually inspected for the correct cut site and successful separation before
614 being transferred to a 60 mm petri dish and incubated in 1:1 $MgCl_2$: FSW for a minimum of 1 hour. The
615 juveniles were then washed into FSW and moved to a 60 mm petri dish containing mud and FSW for 1
616 week. For analysis, juvenile worms were sifted from the mud and placed into a petri dish of FSW. Worms
617 were fixed with 4% paraformaldehyde (PFA) in FSW for 30 min before being washed into phosphate-
618 buffered saline (PBS). Fixed juveniles were scored for pigmented eye cells before being processed for
619 antibody labeling.

620 *2.3 Cell Proliferation Assay*

621 Sibling larvae dissected from a single brood tube were incubated in EdU (Click-iT EdU Alexa Fluor
622 488 imaging kit - Invitrogen) diluted in FSW to a final concentration of 3 uM at room temperature for 30
623 minutes. Larvae were then washed into a 1:1 $MgCl_2$: FSW solution for 10 minutes and then fixed in 4%
624 PFA for 30 minutes. Afterward, they were rinsed into PBS and incubated for 20 minutes at room
625 temperature in PBT (PBS + 0.05% Triton-X-100) with rocking. The specimens were incubated in EdU
626 reaction buffer for 30 minutes, rocking at room temperature. Finally, they were washed into PBS and
627 stored at 4 degrees celsius until needed.

628 *2.4 EdU Quantification*

629 Quantification of EdU and DAPI stained cells was conducted by importing Z-stacks generated
630 from confocal microscopy (see Microscopy) into ImageJ software. Quantification of anterior and
631 posterior amputations were analyzed using the same methodology. Using DAPI and DIC channels to
632 establish boundaries, each image was cropped around the perimeter of the animal. The channels were
633 split and treated separately to optimize cell counting. The threshold for each channel was adjusted
634 manually to minimize background and enhance distinction of individual cells. Afterward, a mask and
635 watershed application were applied to each channel. The resulting image was divided into three equal
636 sections along the anterior-posterior axis using the Montage to Stack application. The modified images
637 were compiled into 20 slice projections (20 µm total) before being counted automatically by the Analyze
638 Particles in the Analyze menu. Each 20 µm Z-stack was counted, with the results automatically
639 summarized via section. Manual inspection eliminated any cells that were counted twice by the
640 software. Results were manually compiled by channel and section for each animal, as well as for each
641 time point. A ratio of EdU stained cells to DAPI stained cells was calculated for each time point from the
642 ImageJ cell count summaries. Averages of each section (anterior, middle, and posterior) for each time

643 point (uncut controls, 6 hpa, 3dpa, and 5dpa) was calculated separately. Each body section of uncut
644 controls was compared with corresponding body sections of amputated animals. One-way weighted
645 ANOVA statistical tests were performed using VassarStats to test for significance between the control
646 and amputation group of interest.

647 *2.5 Antibody labeling and phalloidin staining*

648 Amputated larvae or juveniles were incubated in a 1:1 $MgCl_2$: FSW solution for 10 minutes and fixed in
649 4% paraformaldehyde in FSW for 30 minutes. Animals were washed into PBS and then a PBS+ Triton
650 solution (0.1% Triton-X-100 for larvae and 0.2% Triton-X-100 for juveniles), rocking at room temperature
651 for 45–60 min. For antibody labeling, the anti-acetylated tubulin antibody (goat anti-mouse, Sigma-
652 Aldrich Co.) was diluted 1:400 in block solution (10% heated treated goat serum in PBT), and incubated
653 at room temperature for 2 hours or overnight at 4°C. Following multiple washes in PBT (4 times in PBT
654 for 30 minutes each), a secondary antibody (goat anti-mouse red 594, Invitrogen) was diluted 1:400 in
655 block solution and incubated 2–4 hours rocking at room temperature or overnight at 4°C. The 22C10
656 antibody (Goat anti-mouse, Developmental Studies Hybridoma bank) (22C10 was deposited to the DSHB
657 by Benzer, S. / Colley, N. (DSHB Hybridoma Product 22C10)) was diluted 1:200 in block solution, and
658 incubated overnight at 4°C. Following multiple washes in PBT over two hours, the secondary antibody
659 (goat anti-mouse green 488 - Invitrogen) was diluted 1:400 in block solution and incubated overnight at
660 4°C. Following incubation in secondary antibody, larvae were rinsed 2–3 times in PBT and then washed 4
661 times in PBT for 30 minutes each wash. For phalloidin staining, specimens were transferred to a 3 well
662 glass depression plate and incubated in a 1:400 dilution of phalloidin (Alexa Fluor 488 phalloidin,
663 Invitrogen) in PBT. Specimens were incubated on a rocker at room temperature for 45–60 min before
664 being washed twice in PBT for 30 minutes each wash. Animals were cleared in 80% glycerol in PBS with
665 Hoechst overnight prior to imaging.

666 *2.6 Whole mount in situ hybridization*

667 Larvae collected at different time points following amputation were incubated in a 1:1 $MgCl_2$:
668 FSW solution for 10 minutes and then fixed in 4% paraformaldehyde overnight. Fixative was removed by
669 multiple rinses in PBS and then larvae were gradually washed into 100% methanol and stored at -20°C.
670 Following a previously described protocol (de Jong & Seaver, 2017), whole mount in situ hybridization
671 was performed. DIG-labeled RNA probes were generated with the MegaScript SP6 or T7 Transcription kit
672 (Invitrogen). The following working concentrations and probes were used: *ash1* with 3ng/ul, *MyoD* with
673 0.5ng/ul, *vasa* with 1ng/ul, and *elav* with 2ng/ul. Animals were hybridized for ~24 – 48 hours at 65°C.
674 Each RNA probe was visualized by color reaction with NBT/BCIP and visually monitored. For each
675 sample, uncut control larvae were developed alongside experimental, amputated larvae. The reaction
676 was terminated following washes of PBT followed by a final fixation in 4% PFA in FSW for 30 min. Nuclei
677 were stained with 0.1 ug/ml Hoescht in PBS and 80% glycerol before individuals were placed on
678 microscope slides for analysis and imaging.

679 *2.7 Tissue and Cilia Measurements*

680 To measure tissue formation in amputated larvae, confocal images were analyzed using ImageJ
681 software. Multiple measurements were made on each specimen for the applicable traits. Nervous
682 system measurements were measured from the cut site to the ectoderm distal to the cut site. The
683 muscle measurements were taken from the cut site to the ectoderm distal to the cut site. Changes in
684 body width were calculated by making two measurements per specimen; the first measurement was
685 taken at the axial level of the mouth, and the second was taken just posterior to the cut site. Gut
686 measurements were made from the posterior end of the pigmented gut to the edge of the posterior
687 ectoderm. For anterior amputations the muscle and nervous system were measured in 6 hpa (n = 8) and
688 3 dpa (n = 10) larvae. For posterior amputations, the muscle, nervous system, and changes in body width
689 were measured for 6 dpa (n = 7) and 5 dpa (n = 10). Additionally, the gut was used as a measurement
690 landmark for 5 dpa and Stage 9 larvae at 6 hpa (n = 10). One-way weighted ANOVA statistical tests were
691 performed using *goodcalculators* to test for significance between the control and amputation group of
692 interest.

693 The cilia of larvae were measured using ImageJ software on confocal images. Using the channel
694 in which the cilia are labelled with anti-acetylated tubulin, we traced individual labeled cilia of the
695 prototroch, neurotroch, telotroch, and pygidium. Lines resulting from the trace were then measured
696 using the 'measure' tool found under 'Analyze.' At least three cilia per ciliary band were measured in a
697 representative specimen of a given experimental group.

698 *2.8 Metamorphosis assays*

699 A single multivitamin (Centrum Men Multivitamin) was dissolved in 200 ml FSW. Larvae were
700 placed in a 30mm petri dish in FSW. Most of the FSW was removed from the dish and replaced with 3 ml
701 of the multi-vitamin solution. Animals were left in the vitamin solution for 20 - 30 minutes. Animals were
702 then washed rapidly with FSW (2 ml/wash), a minimum of three times. Animals were individually scored
703 for successful settlement and metamorphosis. Successful settlement and metamorphosis were defined
704 as cessation of swimming behavior and initiation of burrowing, loss of the prototroch and/or telotroch
705 ciliary bands and elongation of the body.

706 *2.9 Microscopy and Imaging*

707 Larvae were imaged with a Zeiss 710 confocal microscope using 4x bidirectional and
708 unidirectional settings for green and red channels. Z-stacks were compiled using ImageJ software
709 (Schindelin et al., 2012). Differential interference contrast microscopy images were captured on a Zeiss
710 AxioSkop II motplus compound microscope (Zeiss) coupled with a SPOT FLEX digital camera (Diagnostic
711 Instruments Inc). Multiple focal planes were merged for DIC images using Helicon Focus software
712 (Helicon Focus 7). Images were processed for brightness, cropping, and contrast with Illustrator (Adobe
713 Illustrator 2020) or or Photoshop (Adobe Photoshop 2020). Figures were composed using Adobe
714 Illustrator (Adobe Illustrator 2020).

715 **Acknowledgements**

716 We thank Brent Foster, Lauren Kunselman, and Katie Feerst for critical reading of the manuscript.

Author Contributions

Conceived and designed the experiments: AAB ECS. Performed the experiments: AAB. Analyzed the data: AAB ECS. Contributed reagents/materials/analysis tools: ECS AAB. Wrote the paper: AAB ECS.

References

Alvarado, A. S. (2000). Regeneration in the metazoans: why does it happen? *BioEssays*. https://doi.org/10.1002/(SICI)1521-1878(200006)22:6

Bely, A. E. (2006). Distribution of segment regeneration ability in the Annelida. *Integrative and Comparative Biology*, *46*(4), 508–518. https://doi.org/10.1093/icb/icj051

Bely, Alexandra E, & Sikes, J. M. (2010). Latent regeneration abilities persist following recent evolutionary loss in asexual annelids. *Proceedings of the National Academy of Sciences of the United States of America*, *107*(4), 1464–1469. https://doi.org/10.1073/pnas.0907931107

Berrill, N. J. (1928). *Regeneration in the polychret Choetopterus Ohcetopterus*. 151–158.

Biggers, W. J., & Laufer, H. (1999). Settlement and Metamorphosis of Capitella Larvae Induced by Juvenile Hormone-Active Compounds Is Mediated by Protein Kinase C and Ion Channels. *Https://Doi.Org/10.2307/1542564*, *196*(2), 187–198. https://doi.org/10.2307/1542564

Biggers, W. J., Pires, A., Pechenik, J. A., Johns, E., Patel, P., Polson, T., & Polson, J. (2012). Inhibitors of nitric oxide synthase induce larval settlement and metamorphosis of the polychaete annelid Capitella teleta. *Invertebrate Reproduction and Development*, *56*(1), 1–13. https://doi.org/10.1080/07924259.2011.588006

Boyle, M. J., & Seaver, E. C. (2008). Developmental expression of foxA and gata genes during gut formation in the polychaete annelid, Capitella sp. I. *Evolution & Development*, *10*(1), 89–105. https://doi.org/10.1111/J.1525-142X.2007.00216.X

Brockes, J. P. (1997). Amphibian Limb Regeneration: Rebuilding a Complex Structure. *Science*, *276*(5309), 81–87. https://doi.org/10.1126/SCIENCE.276.5309.81

Burns, R. T., Pechenik, J. A., Biggers, W. J., Scavo, G., & Lehman, C. (2014). The b vitamins nicotinamide (b>3) and riboflavin (b2) stimulate metamorphosis in larvae of the deposit- Feeding polychaete capitella teleta: Implications for a sensory ligand-gated ion channel. *PLoS ONE*, *9*(11). https://doi.org/10.1371/journal.pone. 0109535

Byrnes, E. F. (1904). Regeneration of the anterior limbs in the tadpoles of frogs. *Archiv Für Entwicklungsmechanik Der Organismen*, *18*(2), 171–177. https://doi.org/10.1007/BF02163652

Carnevali, C. (2006). Regeneration in Echinoderms: repair, regrowth, cloning. In *ISJ* (Vol. 3).

Carnevali, M. D. C., Lucca, E., & Bonasoro, F. (1993). Mechanisms of arm regeneration in the feather star Antedon mediterranea: Healing of wound and early stages of development. *Journal of Experimental Zoology*, *267*(3), 299–317. https://doi.org/10.1002/JEZ.1402670308

Cary, G. A., Wolff, A., Zueva, O., Pattinato, J., & Hinman, V. F. (2019). Analysis of sea star larval regeneration reveals conserved processes of whole-body regeneration across the metazoa. *BMC Biology*, *17*(1), 16. https://doi.org/10.1186/s12915-019-0633-9

Cary, G., & Hinman, V. (2017). Conserved processes of metazoan whole-body regeneration identified in sea star larvae. *BioRxiv*, 118232. https://doi.org/10.1101/118232

Chartier, T. F., Arendt, D., Deschamps, J., Dürichen, W., & Jékely, G. (n.d.). *Whole-head recording of chemosensory activity in the marine annelid Platynereis dumerilii*. https://doi.org/10.1098/rsob.180139

Chartier, T. F., Deschamps, J., Dürichen, W., Jékely, G., & Arendt, D. (2018). Whole-head recording of chemosensory activity in the marine annelid Platynereis dumerilii. *Open Biology*, *8*(10). https://doi.org/10.1098/RSOB.180139

Cohen, R. A., & Pechenik, J. A. (1999). Relationship between sediment organic content, metamorphosis, and postlarval performance in the deposit-feeding polychaete Capitella sp. *Journal of Experimental Marine Biology and Ecology*, *240*, 1–18.

Conzelmann, M., Williams, E. A., Tunaru, S., Randel, N., Shahidi, R., Asadulina, A., Berger, J., Offermanns, S., & Jékely, G. (2013). Conserved MIP receptor-ligand pair regulates Platynereis larval settlement. *Proceedings of the National Academy of Sciences of the United States of America*, *110*(20), 8224–8229. https://doi.org/10.1073/PNAS.1220285110/-/DCSUPPLEMENTAL

Cuvier, G., Cuvier, G., & Latreille, P. A. (1829). Le règne animal distribué d'après son organisation, pour servir de base à l'histoire naturelle des animaux et d'introduction à l'anatomie comparée. In *Le règne animal distribué d'après son organisation, pour servir de base à l'histoire naturelle des animaux et d'introduction à l'anatomie comparée*. Chez Déterville. https://doi.org/10.5962/bhl.title.49223

Dannenberg, L. C., & Seaver, E. C. (2018). Regeneration of the germline in the annelid Capitella teleta. *Developmental Biology*, *440*(2), 74–87. https://doi.org/10.1016/j.ydbio.2018.05.004

de Jong, D. M., & Seaver, E. C. (2016). A Stable Thoracic Hox Code and Epimorphosis Characterize Posterior Regeneration in Capitella teleta. *PLOS ONE*, *11*(2), e0149724. https://doi.org/10.1371/journal.pone.0149724

de Jong, D. M., & Seaver, E. C. (2017). Investigation into the cellular origins of posterior regeneration in the annelid Capitella teleta. *Regeneration (Oxford, England)*, *5*(1), 61–77. https://doi.org/10.1002/reg2.94

Dill, K. K., & Seaver, E. C. (2008). Vasa and nanos are coexpressed in somatic and germ line tissue from early embryonic cleavage stages through adulthood in the polychaete Capitella sp. I. *Development Genes and Evolution*, *218*(9), 453–463. https://doi.org/10.1007/s00427-008-0236-x

Gaire, J., Varholick, J. A., Rana, S., Sunshine, M. D., Doré, S., Barbazuk, W. B., Fuller, D. D., Maden, M., & Simmons, C. S. (2021). Spiny mouse (Acomys): an emerging research organism for regenerative medicine with applications beyond the skin. *Npj Regenerative Medicine 2021 6:1*, *6*(1), 1–6. https://doi.org/10.1038/s41536-020-00111-1

Giani, V. C., Yamaguchi, E., Boyle, M. J., & Seaver, E. C. (2011). Somatic and germline expression of piwi during development and regeneration in the marine polychaete annelid Capitella teleta. *EvoDevo*, *2*(1). https://doi.org/10.1186/2041-9139-2-10

Hadfield, M. G. (2010). Biofilms and Marine Invertebrate Larvae: What Bacteria Produce That Larvae Use to Choose Settlement Sites. *Https://Doi.Org/10.1146/Annurev-Marine-120709-142753*, *3*, 453–470. https://doi.org/10.1146/ANNUREV-MARINE-120709-142753

Hadfield, M. G., Meleshkevitch, E. A., & Boudko, D. Y. (2000). The apical sensory organ of a gastropod veliger is a receptor for settlement cues. *Https://Doi.Org/10.2307/1542804*, *198*(1), 67–76. https://doi.org/10.2307/1542804

Harrison, R. G. (1898). The growth and regeneration of the tail of the frog larva - Studied with the aid of Born's method of grafting. *Archiv Für Entwickelungsmechanik Der Organismen*, *7*(2–3), 430–485.

https://doi.org/10.1007/BF02161494

Hiebert, T. C., & Maslakova, S. (2015). Integrative taxonomy of the Micrura alaskensis Coe, 1901 species complex (Nemertea: Heteronemertea), with descriptions of a new genus maculaura gen. nov. and four new species from the NE pacific. *Zoological Science*, *32*(6), 615–637. https://doi.org/10.2108/ZS150011

Jeffery, W. R. (2015). Regeneration, Stem Cells, and Aging in the Tunicate Ciona: Insights from the Oral Siphon. *International Review of Cell and Molecular Biology*, *319*, 255–282. https://doi.org/10.1016/bs.ircmb.2015.06.005

Juliano, C. E., Swartz, S. Z., & Wessel, G. M. (2010). A conserved germline multipotency program. *Development*, *137*(24), 4113–4126. https://doi.org/10.1242/DEV.047969

Luttrell, S. M., Su, Y. H., & Swalla, B. J. (2018). Getting a head with ptychodera flava larval regeneration. *Biological Bulletin*, *234*(3), 152–164. https://doi.org/10.1086/698510

Meyer, N. P., Boyle, M. J., Martindale, M. Q., & Seaver, E. C. (2010). A comprehensive fate map by intracellular injection of identified blastomeres in the marine polychaete Capitella teleta. *EvoDevo*, *1*(1). https://doi.org/10.1186/2041-9139-1-8

Meyer, N. P., Carrillo-Baltodano, A., Moore, R. E., & Seaver, E. C. (2015). Nervous system development in lecithotrophic larval and juvenile stages of the annelid Capitella teleta. *Frontiers in Zoology*, *12*(1), 1–27. https://doi.org/10.1186/s12983-015-0108-y

Meyer, N. P., & Seaver, E. C. (2009). Neurogenesis in an annelid: Characterization of brain neural precursors in the polychaete Capitella sp. I. *Developmental Biology*, *335*(1), 237–252. https://doi.org/10.1016/J.YDBIO.2009.06.017

Nedved, B. T., Freckelton, M. L., & Hadfield, M. G. (2021). Laser ablation of the apical sensory organ of Hydroides elegans (Polychaeta) does not inhibit detection of metamorphic cues. *The Journal of Experimental Biology*, *224*(20). https://doi.org/10.1242/JEB.242300

Oulhen, N., Heyland, A., Carrier, T. J., Zazueta-Novoa, V., Fresques, T., Laird, J., Onorato, T. M., Janies, D., & Wessel, G. (2016). Regeneration in bipinnaria larvae of the bat star Patiria miniata induces rapid and broad new gene expression. *Mechanisms of Development*, *142*, 10–21. https://doi.org/10.1016/j.mod.2016.08.003

Özpolat, B. D., & Bely, A. E. (2016). Developmental and molecular biology of annelid regeneration: a comparative review of recent studies. *Current Opinion in Genetics & Development*, *40*, 144–153. https://doi.org/10.1016/j.gde.2016.07.010

Pernet, B., Amiel, A., & Seaver, E. C. (2012). Effects of maternal investment on larvae and juveniles of the annelid Capitella teleta determined by experimental reduction of embryo energy content. *Invertebrate Biology*, *131*(2), 82–95. https://doi.org/10.1111/j.1744-7410.2012.00263.x

Phipps, L. S., Marshall, L., Dorey, K., & Amaya, E. (2020). Model systems for regeneration: Xenopus. *Development (Cambridge)*, *147*(6). https://doi.org/10.1242/DEV.180844/223048

Rawls, A., & Olson, E. N. (1997). MyoD meets its maker. *Cell*, *89*(1), 5–8. https://doi.org/10.1016/S0092-8674(00)80175-0

Schindelin, J., Arganda-Carreras, I., Frise, E., Kaynig, V., Longair, M., Pietzsch, T., Preibisch, S., Rueden, C.,

Saalfeld, S., Schmid, B., Tinevez, J. Y., White, D. J., Hartenstein, V., Eliceiri, K., Tomancak, P., & Cardona, A. (2012). Fiji: an open-source platform for biological-image analysis. *Nature Methods 2012 9:7*, *9*(7), 676–682. https://doi.org/10.1038/nmeth.2019

Seaver, E. C. (2022). Sifting through the mud: A tale of building the annelid Capitella teleta for EvoDevo studies. *Current Topics in Developmental Biology*, *147*, 401–432. https://doi.org/10.1016/BS.CTDB.2021.12.018

Seaver, E. C., & De Jong, D. M. (2021). Regeneration in the Segmented Annelid Capitella teleta. *Genes*, 12. https://doi.org/10.3390/genes12111769

Seaver, E. C., Thamm, K., & Hill, S. D. (2005). Growth patterns during segmentation in the two polychaete annelids, Capitella sp. I and Hydroides elegans: comparisons at distinct life history stages. *Evolution Development*, *7*(4), 312–326. https://doi.org/10.1111/j.1525-142X.2005.05037.x

Simakov, O., Marletaz, F., Cho, S. J., Edsinger-Gonzales, E., Havlak, P., Hellsten, U., Kuo, D. H., Larsson, T., Lv, J., Arendt, D., Savage, R., Osoegawa, K., De Jong, P., Grimwood, J., Chapman, J. A., Shapiro, H., Aerts, A., Otillar, R. P., Terry, A. Y., … Rokhsar, D. S. (2013). Insights into bilaterian evolution from three spiralian genomes. In *Nature* (Vol. 493, Issue 7433, pp. 526–531). Nature Publishing Group. https://doi.org/10.1038/nature11696

Singer, M. (1954). Induction of regeneration of the forelimb of the postmetamorphic frog by augmentation of the nerve supply. *Journal of Experimental Zoology*, *126*(3), 419–471. https://doi.org/10.1002/jez.1401260304

Sur, A., Magie, C. R., Seaver, E. C., & Meyer, N. P. (2017). *Spatiotemporal regulation of nervous system development in the annelid Capitella teleta*. *8*, 13. https://doi.org/10.1186/s13227-017-0076-8

Vickery, M. C. L., Vickery, M. S., Amsler, C. D., & Mcclintock, J. B. (2001). Regeneration in Echinoderm Larvae. *Microscopy Research and Technique*, *55*(6), 464–473. https://doi.org/10.1002/jemt.1191

Vickery, M. S., & McClintock, J. B. (1998). Regeneration in metazoan larvae [6]. In *Nature* (Vol. 394, Issue 6689, p. 140). Nature Publishing Group. https://doi.org/10.1038/28086

Vickery, Minako S., Vickery, M. C. L., & McClintock, J. B. (2002). Morphogenesis and organogenesis in the regenerating planktotrophic larvae of asteroids and echinoids. *Biological Bulletin*, *203*(2), 121–133. https://doi.org/10.2307/1543381

Yamaguchi, E., Dannenberg, L. C., Amiel, A. R., & Seaver, E. C. (2016). Regulative capacity for eye formation by first quartet micromeres of the polychaete Capitella teleta. *Developmental Biology*, *410*(1), 119–130. https://doi.org/10.1016/j.ydbio.2015.12.009

Yamaguchi, E., & Seaver, E. C. (2013). The importance of larval eyes in the polychaete Capitella teleta: Effects of larval eye deletion on formation of the adult eye. *Invertebrate Biology*, *132*(4), 352–367. https://doi.org/10.1111/ivb.12034

Zammit, P. S. (2017). Function of the myogenic regulatory factors Myf5, MyoD, Myogenin and MRF4 in skeletal muscle, satellite cells and regenerative myogenesis. *Seminars in Cell & Developmental Biology*, *72*, 19–32. https://doi.org/10.1016/J.SEMCDB.2017.11.011

Zattara, E. E., & Bely, A. E. (2013). Investment choices in post-embryonic development: Quantifying interactions among growth, regeneration, and asexual reproduction in the annelid *Pristina leidyi*. *Journal of Experimental Zoology Part B: Molecular and Developmental Evolution*, *320*(8), 471–488.

880 https://doi.org/10.1002/jez.b.22523

881 Zattara, E. E., & Bely, A. E. (2016). Phylogenetic distribution of regeneration and asexual reproduction in
882 Annelida: regeneration is ancestral and fission evolves in regenerative clades. *Invertebrate Biology*,
883 *135*(4), 400–414. https://doi.org/10.1111/IVB.12151

884

885 **Figure Legends**

886 Figure 1. Regenerating juveniles and larvae of *C. teleta*. All images are oriented in ventral view with
887 anterior to the left. **A**, **B**, and **C** are images of the posterior end of a regenerating juvenile 3 days post-
888 amputation (dpa) and are from the same specimen. **A** Differential interference contrast (DIC) image
889 showing regeneration of new tissue in juveniles. **B** Nervous system visualized with anti-acetylated
890 tubulin antibody labeling. **C** Phalloidin staining shows muscle fibers with few in regenerating tissue . **D**
891 Stage 6 larva. **E** Stage 9 larva. (G) gut, (N) neural projection, (CM) circular muscle, (Ey) eye, (Pt)
892 prototroch, (Tt) telotroch, (Py) pygidium. The white dotted lines indicate amputation sites. The asterisk
893 marks the position of the mouth. N denotes the number of animals scored that resemble the image
894 shown.

895 Figure 2. Amputated larvae undergo successful wound healing. All images are oriented in ventral view
896 with anterior to the left. Arrows indicate the continuous layer of epithelium, indicative of successful
897 would healing. **A** Stage 6 uncut larva showing experiment design for amputations. The dotted lines
898 indicate cut sites: (AA) anterior amputation and (PA) posterior amputation. **B** Stage 6 larva 6 hpa
899 anterior amputation. **C** Stage 6 larva 6 hpa posterior amputation. **D** Larva 3 dpa anterior amputation. **E**
900 Stage 9 larva 2 dpa anterior amputation. **F** Stage 9 larva 6hpa posterior amputation. The black bracket
901 represents the tissue between the gut and ectoderm. Amputation site is indicated by the black dotted
902 line. N denotes the number of animals scored that resembled the image in the panel. Scale bar is 50 µm.

903 Figure 3. Localized cell proliferation near the amputation site in larvae. All images are oriented in ventral
904 view with anterior to the left. Animals were exposed to EdU to label dividing cells. EdU+ cells are in
905 green. **A–D** are uncut controls: **A** Stage 6, **B** Stage 7, **C** Stage 8, and **D** Stage 9. **E–H** are anterior
906 amputations: **E** 6 hpa, **F** 1 dpa, **G** 3 dpa, and **H** 5 dpa. **I–L** are posterior amputations: **I** 6 hpa, **J** 1 dpa, **K** 3
907 dpa, and **L** 5 dpa. **M**, **N** Quantification of EdU incorporation in anterior (M) and posterior (N)
908 amputations and comparison with uncut controls. Time after amputation is on the X-axis and the ratio of
909 EdU/DAPI cells is on the Y-axis. The white arrows indicate EdU+ cells near the wound site.
910 Developmental stage or time post-amputation is indicated in the bottom left corner of each panel. N
911 denotes the number of animals scored that resemble the image shown. Dark blue represents uncut
912 controls and light blue represents amputated animals. Asterisk denotes significance with $p < 0.05$. Scale
913 bar is 50 µm.

914 Figure 4. *Vasa* is expressed at the wound site in amputated larvae. All images are oriented in ventral
915 view with anterior to the left. The purple coloration indicates localization of *vasa* transcripts by in situ
916 hybridization. **A**, **B**, and **C** *Vasa* expression patterns in uncut larvae at Stage 6, Stage 8, and Stage 9. **D**, **E**,
917 and **F** are anterior larval amputations. **G**, **H**, and **I** are posterior larval amputations. **D** and **G** are
918 amputated larvae 6 hpa (D) and 2 hpa (**G)**. **E** De novo expression is observed in anterior amputations at 2
919 dpa, as indicated by the arrow and is no longer detectable by 5 dpa (**F)**. In posterior amputations,
920 expression near the wound site is observed at both 2 dpa (**H**) and 3 dpa (**I**), as indicated by arrows. The

921 time post-amputation is indicated in the bottom left corner of each panel in D–I. N denotes the number
922 of animals scored that resemble the image shown. (FG) foregut, (MPC) multi-progenitor cell cluster,
923 (PGZ) posterior growth zone. Scale bar is 50 μm.

924 Figure 5. Tissue response to amputation. **A–B"** and **E–I"** are oriented in ventral view. **C–D"** are oriented
925 in lateral view. In all images, anterior is to the left. **A** uncut Stage 6 larva labeled with anti-acetylated
926 tubulin to visualize the nervous system and ciliary bands. **B, C, D, H, I** larvae are labeled with anti-
927 acetylated tubulin (red) and phalloidin (green) showing the nervous system and musculature,
928 respectively. **B**, **B'**, and **B"** are the same specimen. **B** Nervous system and musculature in a larva 2 dpa.
929 **B'** magnified view of posterior wound site showing few muscle fibers distal to cut site. **B"** magnified view
930 of posterior wound site showing fibers in the tissue distal to the amputation site (arrows). **C** larva 6 hpa
931 after anterior amputation. **D**, **D'** and **D"** are the same specimen, 3 dpa anterior amputation. **D'** magnified
932 view of muscle fibers as marked by phalloidin. **D"** magnified view of anti-acetylated tubulin labeling. **E**
933 and **E'** are the same larva 6 hpa labeled with anti-acetylated tubulin; **E'** as a magnification of **E**. **F** and **G**
934 are separate 2 dpa posterior amputated larvae. **F** neural fibers are present distal to the cut site (arrow).
935 **G** shows a specimen lacking neural fibers distal to the cut site. **H** 6 hpa posterior amputation. **I**, **I'**, and **I"**
936 are the same individual at 5 dpa posterior amputation. **I'** longitudinal and circular muscles are present
937 distal to the cut site (arrow). **I"** neurites distal to the cut site (arrow). White brackets in **I'** and **I"** indicate
938 tissue distal to the amputation site. N denotes the number of animals scored that resemble the
939 representative image. Amputation site is indicated by a white dotted line. (VNC) ventral nerve cord, (PN)
940 peripheral nerves. Scale bar is 50 μm.

941 Figure 6. Amputation induces *ash1* but not *elav* expression at the anterior wound site. All images are
942 oriented with anterior to the left. **A-E** are ventral views and **F-I** are lateral views. The purple coloration
943 indicates expression of either *ash1* (**A-E**) or *elav* (**F-I**) transcripts by in situ hybridization. **C-E** and **H-I** are
944 anterior amputations. **A** Stage 6 uncut control. **B** Stage 9 uncut control. **C** 6 hpa. **D** and **E** are the same 3
945 dpa individual. Vertical arrows indicate novel *ash1* ectodermal expression. The boundary between
946 ectodermal and mesodermal layers is indicated by a black dotted line. **F** Stage 6 and **G** Stage 9 uncut
947 controls. **H** 6 hpa. **I** 3 dpa. (Br) brain, (FG) foregut, (VNC) ventral nerve cord. N denotes the number of
948 animals scored that resemble the image indicated. Scale bar is 50 μm.

949 Figure 7. Amputation induces ectopic expression of the myogenesis marker *MyoD*. All images are
950 oriented in ventral view with anterior to the left. *MyoD* expression is visualized by the purple coloration
951 via in situ hybridization. **A** Stage 6 and **B** Stage 9 uncut controls. *MyoD* is expressed in the posterior
952 trunk mesoderm. **C** and **D** are anterior amputations (ant amp). **C** 6 hpa. **D** anterior shift in *MyoD*
953 expression is observed at 7 dpa. **E** 6 hpa posterior amputation (post amp). Spots of staining anterior to
954 the bracket is nonspecific trapping in the chaetae. **F** *MyoD* is expressed along the length of the body in 3
955 dpa animals (compare with E). Brackets indicate the boundaries of detectable *MyoD* expression along
956 the anterior-posterior axis. Amputation sites are indicated by black dotted lines. N denotes the number
957 of animals scored that resemble the representative image. Scale bar is 50 μm.

958 Figure 8. Eye reformation following anterior amputation. All images are oriented with anterior to the
959 left. **A** – **D** are ventral views. **A** DIC image of the anterior end of a Stage 9 uncut larva. **B** DIC image of the
960 anterior end of a larva 5 days after anterior amputation. Image shown is a merge of multiple focal
961 planes. The pigmented cells (PC) of the eye are indicated by arrows. **C**–**F** eye sensory cells (SC, white
962 arrows), labeled by the 22C10 antibody (green). **C** Uncut Stage 9 control. **D** anterior amputated larva 5

963 dpa. **E** and **F** are juvenile worms in lateral view. **E** uncut 2 week-old juvenile and **F** juvenile 1 week post-
964 amputation of the head. **G** Table displaying the number of pigment cells, sensory cells, or either cell
965 (total) present in anteriorly amputated larvae at 6 hpa and 3 dpa or later. Dotted line indicates the
966 outline of the animal. (MG) midgut.

967 Figure 9. Rare reformation of cilia occurs in amputated larvae. Animals are labelled with anti-acetylated
968 tubulin (white). All images are oriented in with anterior to the left. **A** and **D** are uncut controls, oriented
969 in ventral view. **A** Stage 6 uncut larva. **D** Stage 9 uncut larva. **B** and **E** are anterior amputations oriented
970 in lateral view, with anterior to the left. **B** larva 6 hpa. **E** larva 5 dpa with short cilia visible distal to the
971 cut site (arrow). **C** and **F** are posterior amputations in ventral view. **C** larva 6 hpa. **F** larva 5 dpa with both
972 long cilia (LC) and short cilia (SC) distal to the cut site (arrows). (LC) long cilia, (SC) short cilia, (NT)
973 neurotroch, (PT) prototroch, (PYG) pygidium, (TT) telotroch. N denotes the number of animals scored
974 that are similar to the image represented. Amputation site is indicated by the white dotted line. Scale
975 bar is 50 µm.

976 Figure 10. Induction of metamorphosis in amputated larvae. All images are oriented in ventral view with
977 anterior to the left. **A** Uncut Stage 9 larva not exposed to the metamorphic cue. **B** Uncut Stage 9 larva 2
978 hr after inducement with metamorphic cue. **C** anteriorly amputated larva not exposed to metamorphic
979 cue. **D** anteriorly amputated larva 2 hr after exposure to metamorphic cue. **E** posteriorly amputated
980 larva not exposed to metamorphic cue. **F** posteriorly amputated larva 2 hr after exposure to
981 metamorphic cue. (Br) brain, (Ph) pharynx, (Pt) prototroch, and (Tt) telotroch. N denotes the number of
982 animals scored that are similar to the image shown. All images have the same magnification; scale bar
983 50 µm.

984

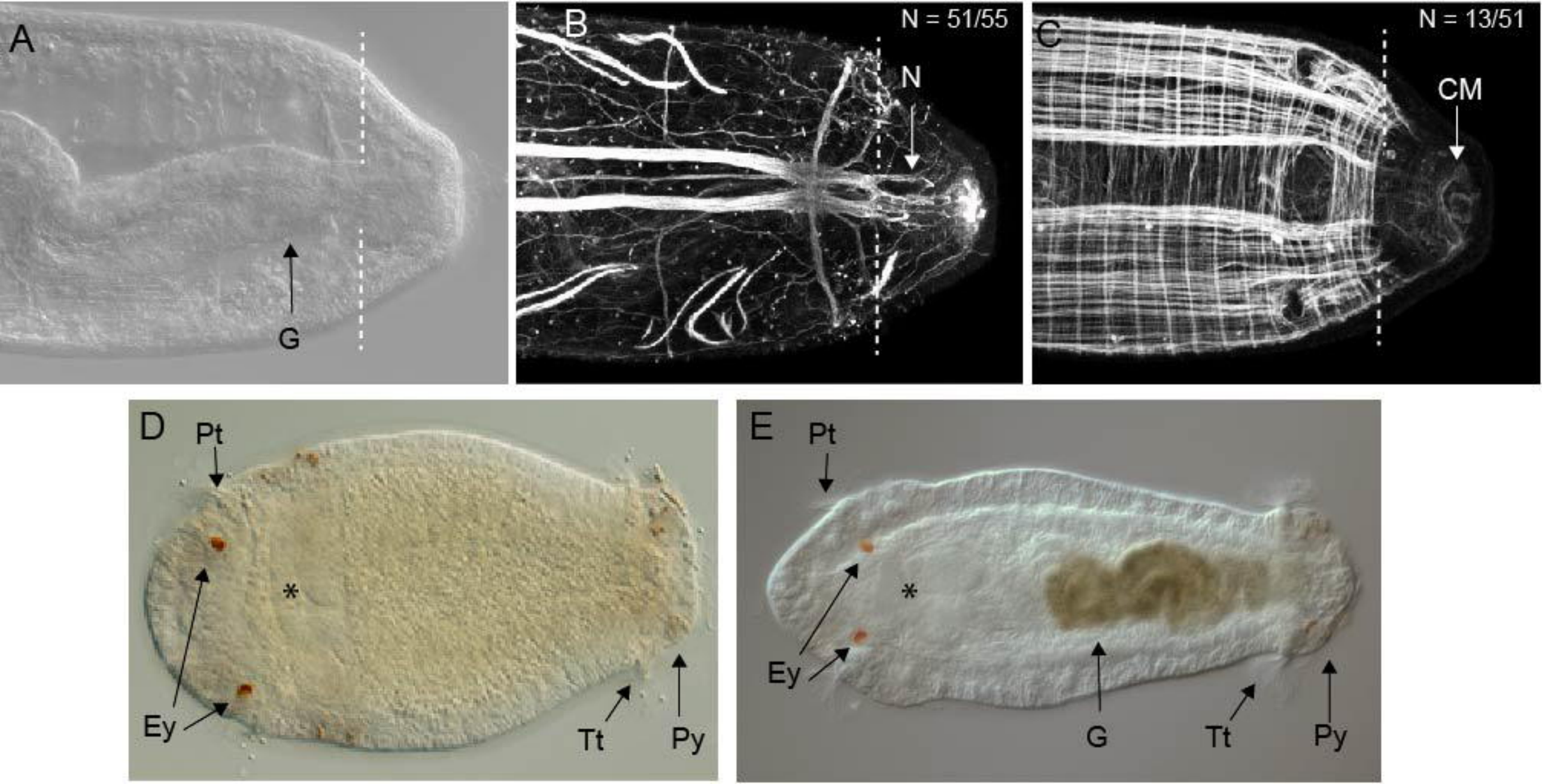
A
G
B
N = 51/55
N
C
N = 13/51
CM
D
Pt
Ey
Tt
Py
E
Pt
Ey
G
Tt
Py

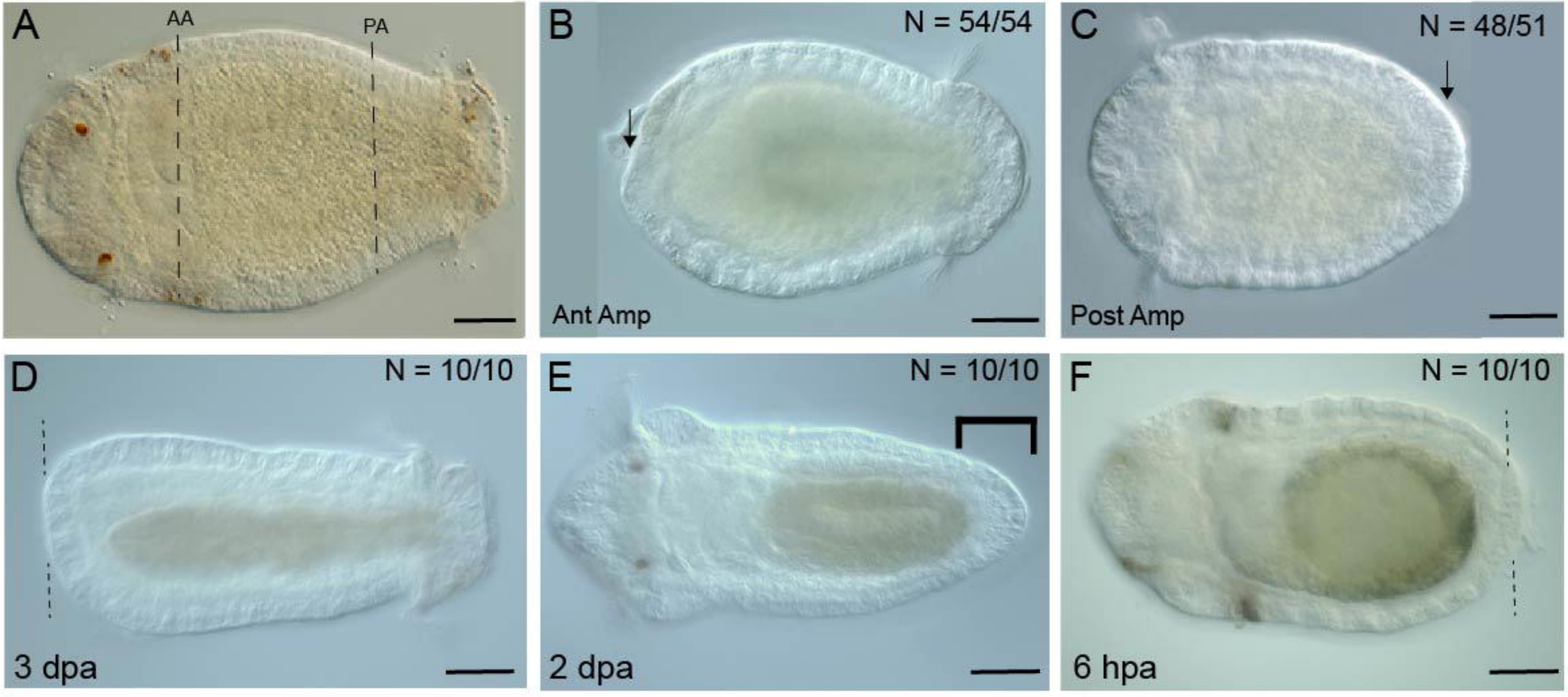
A
AA
PA
B
N = 54/54
Ant Amp
C
N = 48/51
Post Amp
D
N = 10/10
3 dpa
E
N = 10/10
2 dpa
F
N = 10/10
6 hpa

St 6 | 1 dpa | 3 dpa | 5 dpa

Uncut Con

A N = 14/14 St 6

B N = 8/8 St 7

C N = 13/13 St 9

D N = 13/13 St 9

Ant Amp

E N = 19/19 6 hpa

F N = 4/4 1 dpa

G N = 22/22 3 dpa

H N = 19/19 5 dpa

Post Amp

I N = 10/10 6 hpa

J N = 15/15 1 dpa

K N = 15/15 3 dpa

L N = 10/10 5 dpa

M

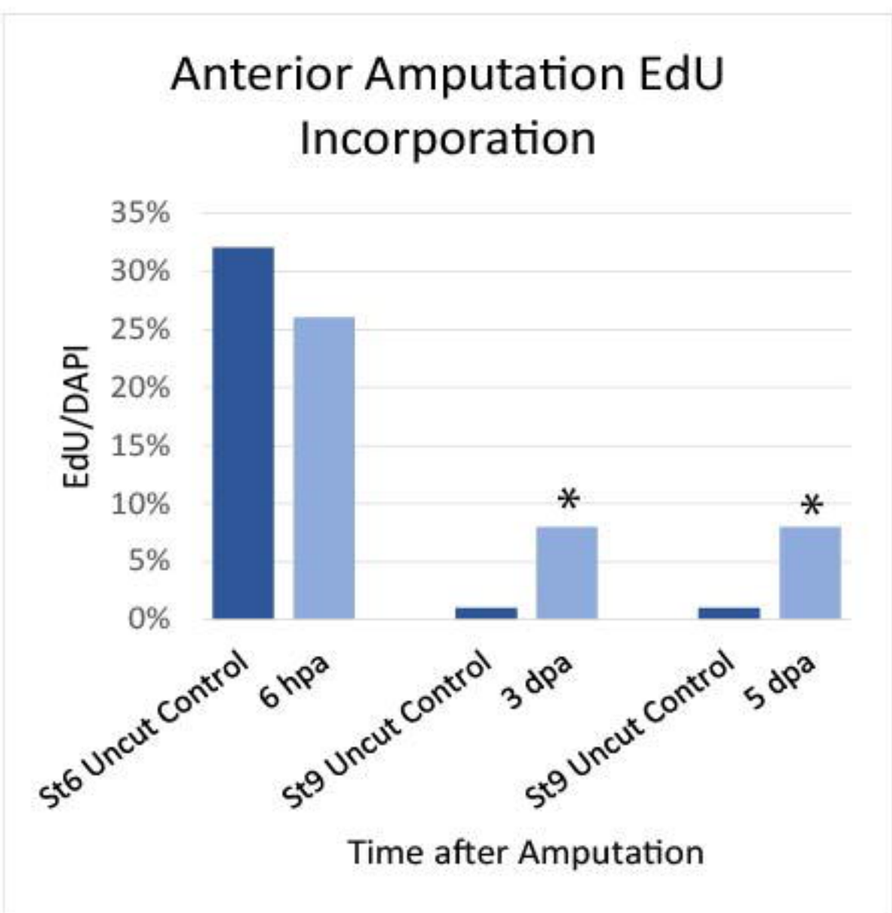

N

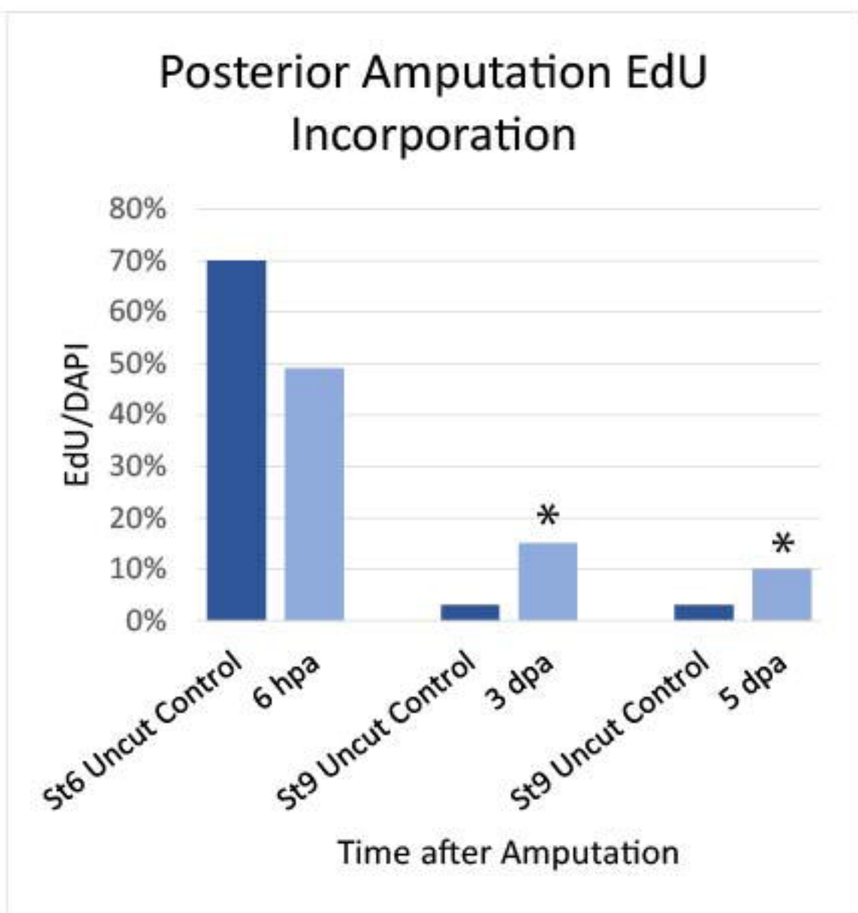

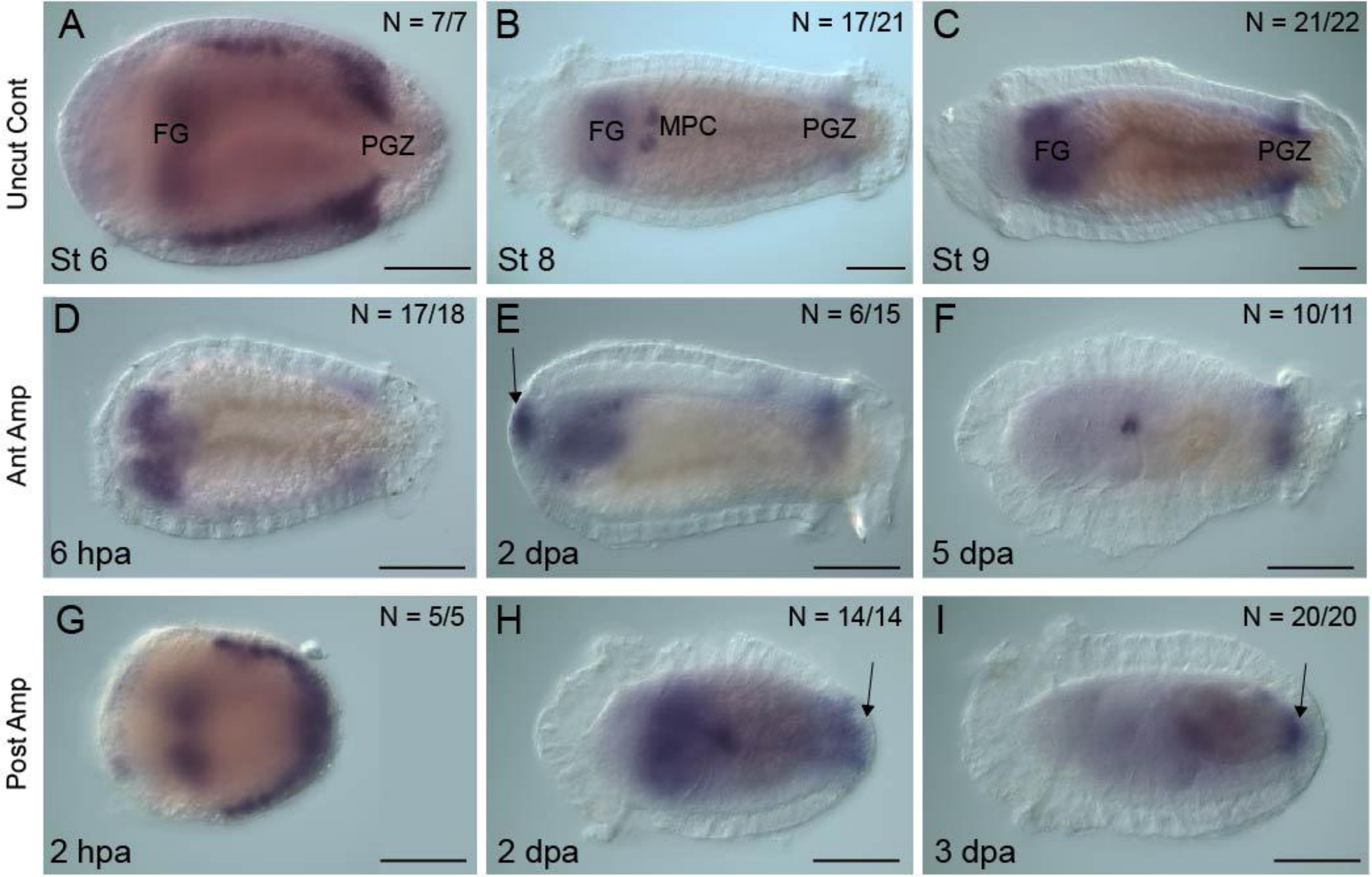
Uncut Cont
Ant Amp
Post Amp
A
N = 7/7
FG
PGZ
St 6
B
N = 17/21
FG
MPC
PGZ
St 8
C
N = 21/22
FG
PGZ
St 9
D
N = 17/18
6 hpa
E
N = 6/15
2 dpa
F
N = 10/11
5 dpa
G
N = 5/5
2 hpa
H
N = 14/14
2 dpa
I
N = 20/20
3 dpa

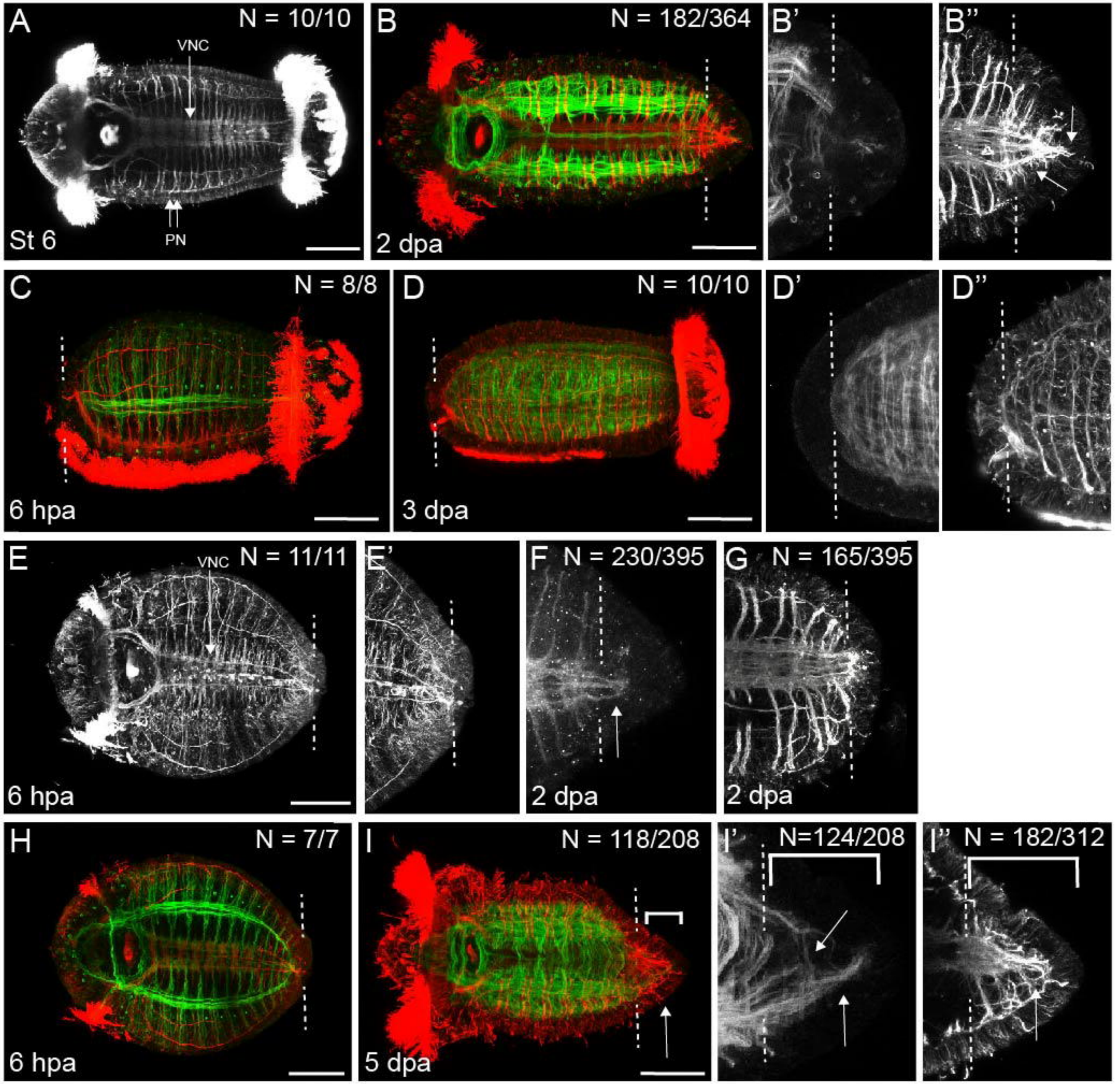
A
N = 10/10
VNC
PN
St 6
B
N = 182/364
2 dpa
B'
B''
C
N = 8/8
6 hpa
D
N = 10/10
3 dpa
D'
D''
E
VNC
N = 11/11
6 hpa
E'
F
N = 230/395
2 dpa
G
N = 165/395
2 dpa
H
N = 7/7
6 hpa
I
N = 118/208
5 dpa
I'
N=124/208
I''
N = 182/312

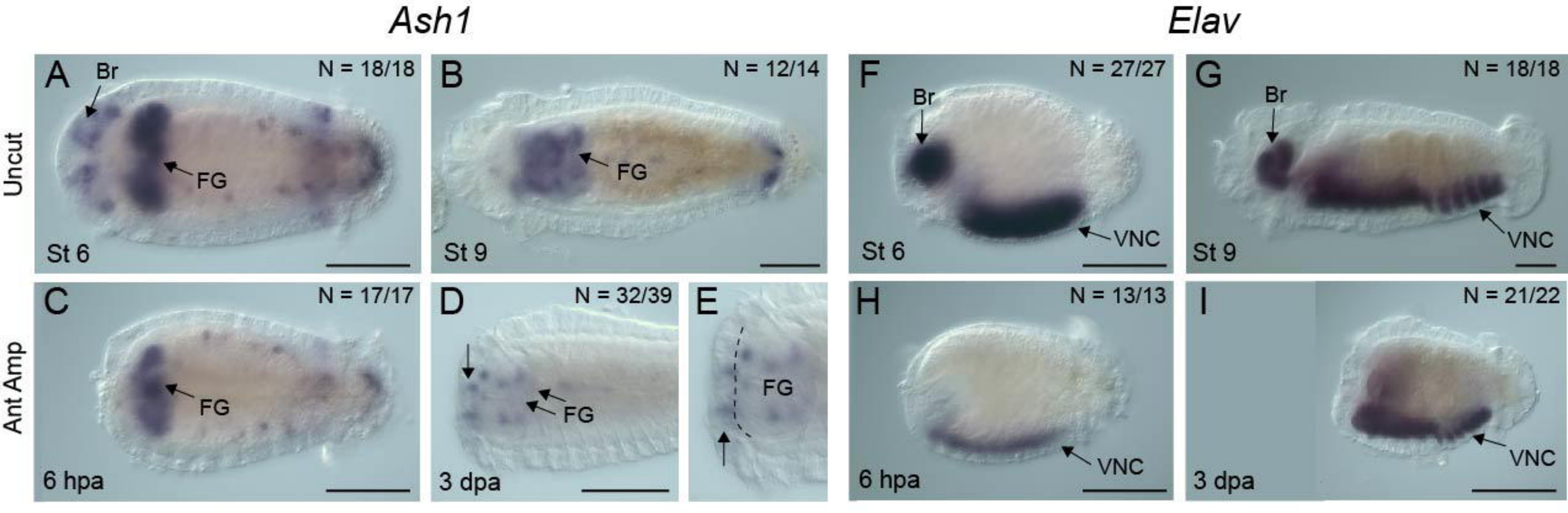
Ash1
Elav
Uncut
Ant Amp
A
Br
FG
N = 18/18
St 6
B
FG
N = 12/14
St 9
F
Br
VNC
N = 27/27
St 6
G
Br
VNC
N = 18/18
St 9
C
FG
N = 17/17
6 hpa
D
FG
N = 32/39
3 dpa
E
FG
H
VNC
N = 13/13
6 hpa
I
VNC
N = 21/22
3 dpa

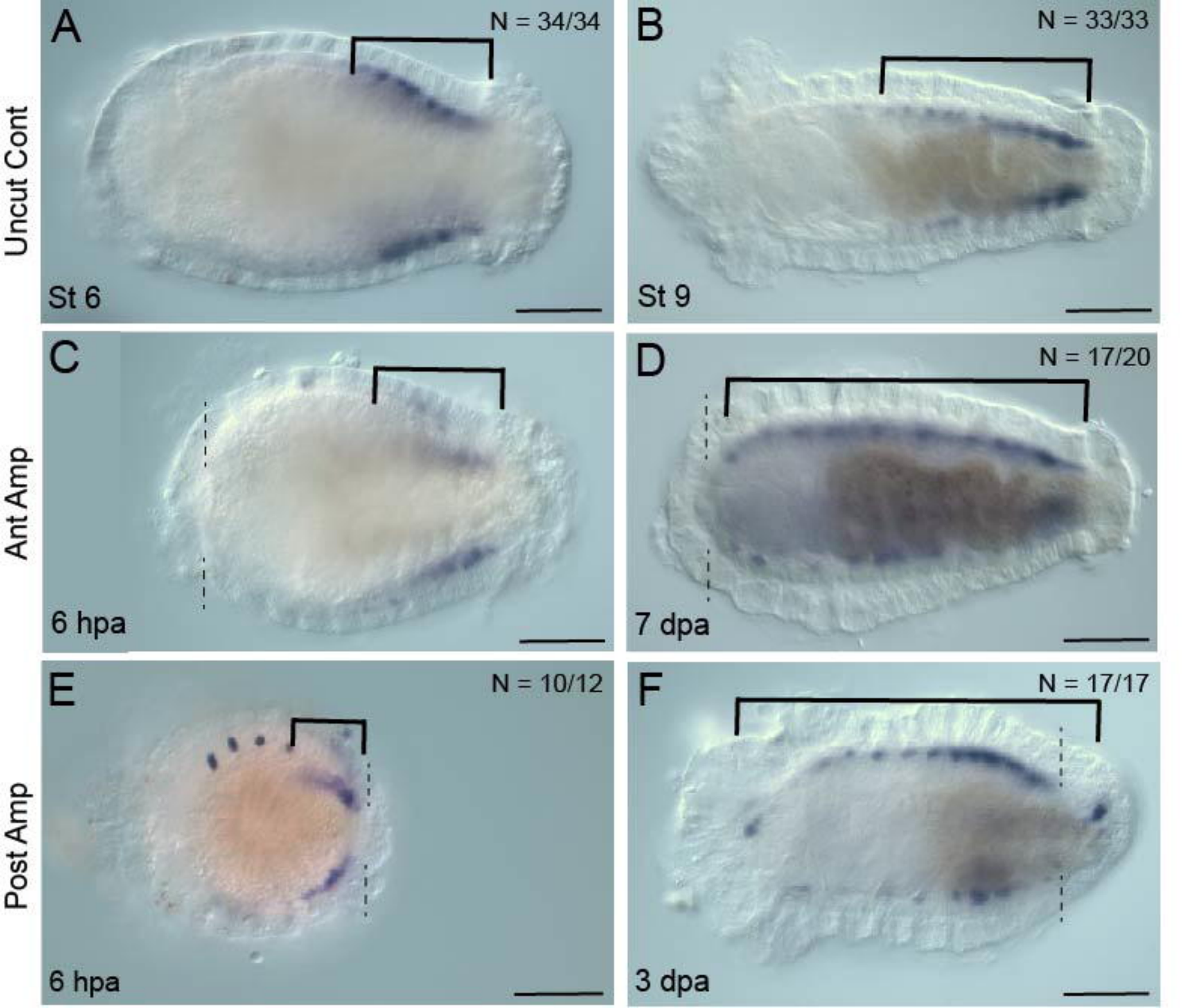
Uncut Cont
A
N = 34/34
St 6
B
N = 33/33
St 9
Ant Amp
C
6 hpa
D
N = 17/20
7 dpa
Post Amp
E
N = 10/12
6 hpa
F
N = 17/17
3 dpa

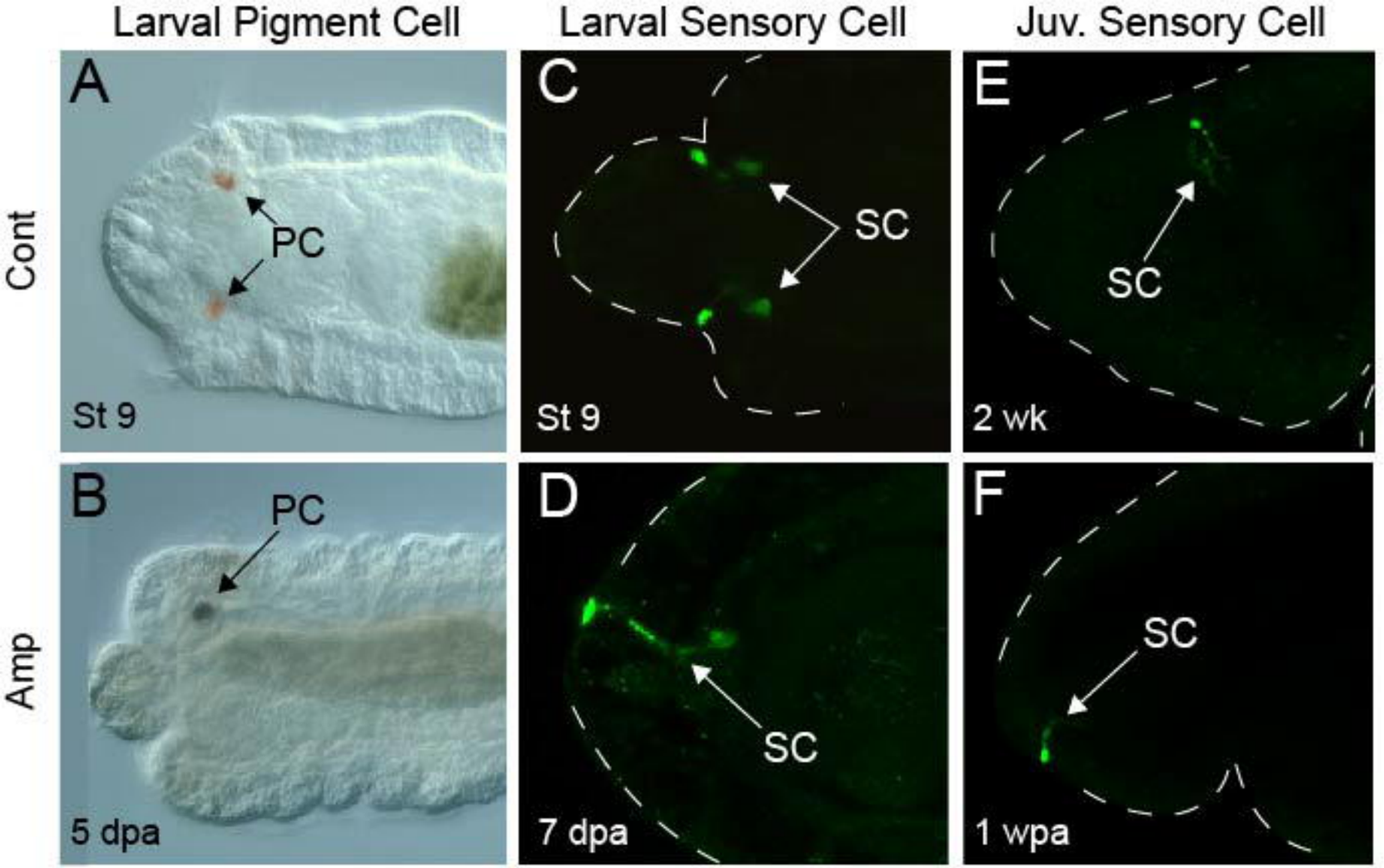

G

	Pigment Cell	Sensory Cell	Total
6 hpa	0/46	0/31	0/57
3 dpa +	28/420	8/220	36/640
	7%	4%	6%

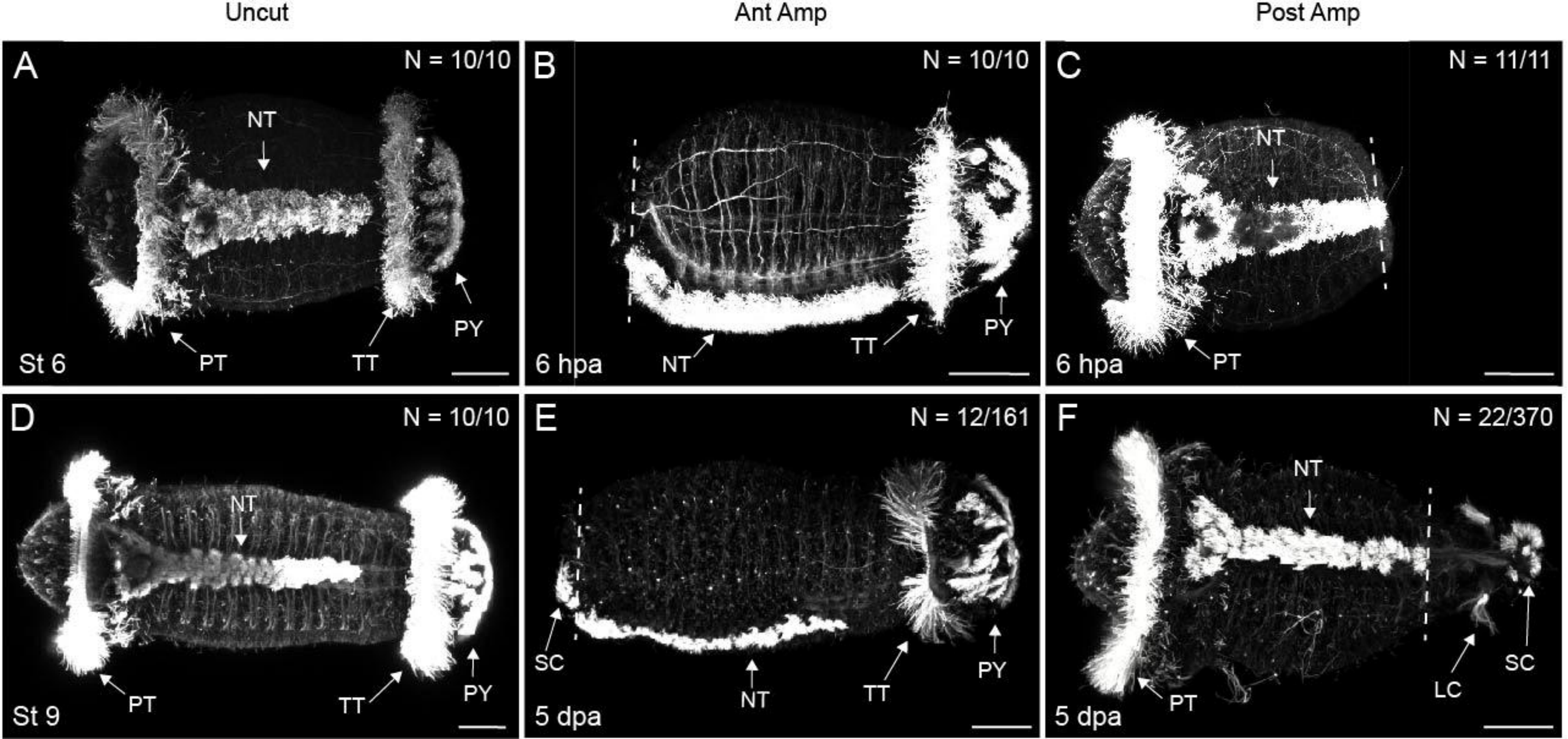
Uncut
Ant Amp
Post Amp
A
N = 10/10
NT
PT
TT
PY
St 6
B
N = 10/10
NT
TT
PY
6 hpa
C
N = 11/11
NT
PT
6 hpa
D
N = 10/10
NT
PT
TT
PY
St 9
E
N = 12/161
SC
NT
TT
PY
5 dpa
F
N = 22/370
NT
PT
LC
SC
5 dpa

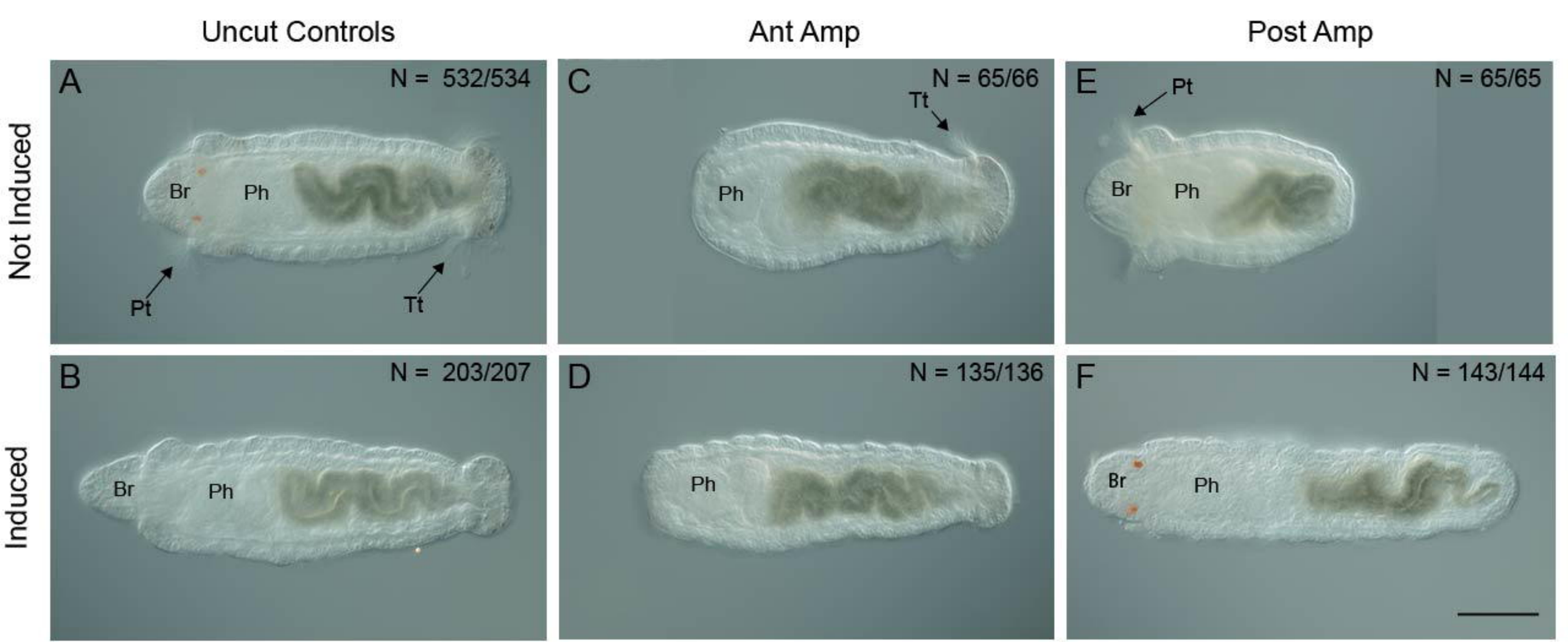
Uncut Controls
Ant Amp
Post Amp
Not Induced
Induced
A
N = 532/534
Br
Ph
Pt
Tt
B
N = 203/207
Br
Ph
C
N = 65/66
Tt
Ph
D
N = 135/136
Ph
E
N = 65/65
Pt
Br
Ph
F
N = 143/144
Br
Ph

Table 1. Quantification of EdU+ cells in anteriorly amputated larvae

Anterior Amp		Anterior		Middle		Posterior	
		Uncut	Cut	Uncut	Cut	Uncut	Cut
6 hpa	# Nuclei	418	392	1216	417	551	250
	# EdU	133	102	466	235	387	136
	%	32%	26%	38%	56%	70%	54%
3 dpa	# Nuclei	447	363	856	457	413	185
	# EdU	3	29	18	2	14	24
	%	1%	8%	2%	0%	3%	13%
5dpa	# Nuclei	147	359	856	516	413	219
	# EdU	3	28	18	5	14	10
	%	2%	8%	2%	1%	3%	5%

Table 2. Quantification of EdU+ cells in posteriorly amputated larvae

Posterior Amp		Anterior		Middle		Posterior	
		Uncut	Cut	Uncut	Cut	Uncut	Cut
6 hpa	# Nuclei	418	155	1216	556	551	463
	# EdU	133	70	466	217	387	225
	%	32%	45%	38%	39%	70%	49%
3 dpa	# Nuclei	447	306	856	702	413	525
	# EdU	3	2	18	6	14	78
	%	1%	1%	2%	1%	3%	15%
5dpa	# Nuclei	147	331	856	547	413	513
	# EdU	3	0	18	0	14	51
	%	2%	0%	2%	0%	3%	10%

Table 3. Amputated larvae measured for tissue distal to cut site

		Muscle	Nervous System	Gut	Width 2 /Width 1
Ant Amp	**6 hpa**	19μm	18μm	N/A	N/A
	3 dpa	22μm	15μm	N/A	N/A
Post Amp	**6 hpa**	* 17μm	* 12μm	N/A	* 0.675
	5 dpa	* 62μm	* 67μm	45μm	* 0.453
	St 9 6 hpa	N/A	N/A	37μm	N/A

* = significance, $p < .05$